



Selectivity of (±)-citalopram at nicotinic acetylcholine receptors and different inhibitory mechanisms between habenular $\alpha3\beta4^*$ and $\alpha9\alpha10$ subtypes

Hugo R. Arias^{a,**}, Xiao-Tao Jin^b, Sofía Gallino^c, Can Peng^b, Dominik Feuerbach^d,
 Jesús García-Colunga^e, Ana Belén Elgoyhen^{c,f}, Ryan M. Drenan^{b,1}, Marcelo O. Ortells^{g,*}

^a Department of Pharmacology and Physiology, College of Osteopathic Medicine, Oklahoma State University Center for Health Sciences, Tahlequah, OK, USA

^b Department of Pharmacology, Northwestern University Feinberg School of Medicine, Chicago, IL, USA

^c Instituto de Investigaciones en Ingeniería Genética y Biología Molecular, Dr. Héctor N. Torres, CONICET, Universidad de Buenos Aires, Argentina

^f Instituto de Farmacología, Facultad de Medicina, Universidad de Buenos Aires, Argentina

^d Novartis Institutes for Biomedical Research, Basel, Switzerland

^e Departamento de Neurobiología Celular y Molecular, Instituto de Neurobiología, Universidad Nacional Autónoma de México, Querétaro, Mexico

^g Facultad de Medicina, Universidad de Morón, Morón and CONICET, Argentina

ARTICLE INFO

Keywords:

Nicotinic acetylcholine receptor
 (±)-Citalopram
 Selective serotonin reuptake inhibitor
 Medial habenula
 Brain slices

ABSTRACT

The inhibitory activity of (±)-citalopram on human (h) $\alpha3\beta4$, $\alpha4\beta2$, and $\alpha7$ nicotinic acetylcholine receptors (AChRs) was determined by Ca^{2+} influx assays, whereas its effect on rat $\alpha9\alpha10$ and mouse habenular $\alpha3\beta4^*$ AChRs by electrophysiological recordings. The Ca^{2+} influx results clearly establish that (±)-citalopram inhibits (IC_{50} 's in μM) $h\alpha3\beta4$ AChRs (5.1 ± 1.3) with higher potency than that for $h\alpha7$ (18.8 ± 1.1) and $h\alpha4\beta2$ (19.1 ± 4.2) AChRs. This is in agreement with the [3H]imipramine competition binding results indicating that (±)-citalopram binds to imipramine sites at desensitized $h\alpha3\beta4$ with > 2-fold higher affinity than that for $h\alpha4\beta2$. The electrophysiological, molecular docking, and *in silico* mutation results indicate that (±)-citalopram competitively inhibits $\alpha9\alpha10$ AChRs (7.5 ± 0.9) in a voltage-independent manner by interacting mainly with orthosteric sites, whereas it inhibits a homogeneous population of $\alpha3\beta4^*$ AChRs at MHB (VI) neurons (7.6 ± 1.0) in a voltage-dependent manner by interacting mainly with a luminal site located in the middle of the ion channel, overlapping the imipramine site, which suggests an ion channel blocking mechanism. In conclusion, (±)-citalopram inhibits $\alpha3\beta4$ and $\alpha9\alpha10$ AChRs with higher potency compared to other AChRs but by different mechanisms. (±)-Citalopram also inhibits habenular $\alpha3\beta4^*$ AChRs, supporting the notion that these receptors are important endogenous targets related to their anti-addictive activities.

1. Introduction

(±)-Citalopram is a selective serotonin reuptake inhibitor (SSRI) used for the treatment of depressive disorders (Varia and Rauscher, 2002), and off-label for alcohol withdrawal (Angelone et al., 1998) and hot flashes as well as eating, anxiety, premenstrual dysphoria, and post-

traumatic stress disorders. In several European countries, (±)-citalopram is also approved for panic and obsessive-compulsive disorders (Stein et al., 2001).

In addition to being able to selectively inhibit serotonin transporters, SSRIs behave as noncompetitive antagonists (NCAs) of several nicotinic acetylcholine receptors (AChRs) (reviewed in (García-Colunga

Abbreviations: AChR, nicotinic acetylcholine receptor; SSRI, selective serotonin reuptake inhibitor; ACh, acetylcholine; NCA, noncompetitive antagonist; RT, room temperature; MHB, medial habenula; VI, ventral inferior; K_i , inhibition constant; K_d , dissociation constant; IC_{50} , ligand concentration that produces 50% inhibition of binding (or of agonist activation); EC_{50} , agonist concentration that produces 50% receptor activation; n_H , Hill coefficient; r^2 , goodness-of-fit for the linear regression; DMEM, Dulbecco's Modified Eagle Medium; BSA, bovine serum albumin; HBSS, HEPES-buffered salt solution; (±)-citalopram, 1-[3-(dimethylamino)propyl]-1-(4-fluorophenyl)-1,3-dihydro-5-isobenzofurancarbonitrile

* Corresponding author. Facultad de Medicina, Universidad de Morón, and CONICET, Machado 914, 4° Piso, Morón, Argentina.

** Corresponding author. Department of Pharmacology and Physiology, College of Osteopathic Medicine, Oklahoma State University Center for Health Sciences, Tahlequah, OK, 74107, USA.

E-mail addresses: hugo.arias@okstate.edu (H.R. Arias), mortells@retina.ar (M.O. Ortells).

¹ Present address: Department of Physiology & Pharmacology, Wake Forest University Health Sciences, 115 S Chestnut St., Winston-Salem, NC 27101.

<https://doi.org/10.1016/j.neuint.2019.104552>

Received 10 July 2019; Received in revised form 11 September 2019; Accepted 20 September 2019

Available online 20 September 2019

0197-0186/© 2019 Elsevier Ltd. All rights reserved.

et al., 2016). The majority work on this area have concerned SSRIs such as fluoxetine, paroxetine, and sertraline (Andreasen et al., 2011a; Arias et al., 2010a; Fryer and Lukas, 1999; Garcia-Colunga et al., 1997), whereas there is less data on (±)-citalopram, especially on its interaction with $\alpha 9\alpha 10$ AChRs. The most compelling evidence that (±)-citalopram modulates AChR activity is based on animal studies indicating that non-selective (e.g., nicotine) (Popik et al., 2003) and $\alpha 7$ -selective (e.g., PNU-282987) agonists (Andreasen et al., 2012, 2011b) enhance the activity of this antidepressant. These results are in agreement with the hypercholinergic hypothesis of depression, where an excessive cholinergic tone over the noradrenergic system may develop in depressive states, and consequently antidepressant-induced AChR inhibition could be part of their mechanisms of action [reviewed in (Arias et al., 2014; García-Colunga et al., 2016; Mineur and Picciotto, 2010)]. The observation of a higher rate of smoking in depressed patients compared to the general population also supports this hypothesis [reviewed in (Mineur and Picciotto, 2010)].

A first attempt to establish whether there is a relationship between (±)-citalopram's clinical effects and its AChR selectivity is to determine the activity of this antidepressant at different AChR subtypes. For example, inhibition of $\alpha 3\beta 4$ -containing ($\alpha 3\beta 4^*$) AChRs expressed in the habenulo-interpeduncular cholinergic pathway might be related to the beneficial activity of (±)-citalopram to alleviate depression (Varia and Rauscher, 2002) and/or alcohol withdrawal (Angelone et al., 1998). Habenular $\alpha 3\beta 4^*$ AChRs are considered important targets for several anti-addictive compounds (Glick et al., 2002; Maisonneuve and Glick, 2003; McCallum et al., 2012). Compounds with relatively higher selectivity for this receptor subtype such as 18-methoxyconaridine (Arias et al., 2017) have anti-addictive properties and decrease alcohol intake in rodents (Rezvani et al., 2016), whereas bupropion and mecamylamine have antidepressant activity (Arias et al., 2018a, 2014). Nevertheless, no direct evidence of (±)-citalopram-induced habenular $\alpha 3\beta 4^*$ AChRs inhibition has been demonstrated so far. In this regard, we sought to determine the selectivity of (±)-citalopram for different AChR subtypes, and its activity on MHb by electrophysiology recordings of ventral inferior (VI) MHb neurons that strongly express $\alpha 3\beta 4^*$ AChRs (Quick et al., 1999; Shih et al., 2014). To further determine its mechanisms of action, the interaction of (±)-citalopram with imipramine sites at $\alpha 3\beta 4$ and $\alpha 4\beta 2$ AChRs is compared by radioligand competition binding experiments, whereas the functional and structural interactions with $\alpha 3\beta 4$ AChRs is respectively resolved by voltage-dependence and molecular docking studies.

A correlation between ligand-induced $\alpha 9\alpha 10$ AChR inhibition and anti-pain and anti-inflammatory activity has been observed (McIntosh et al., 2009; Romero et al., 2017). Since these AChRs are not expressed in the brain (Elgoyhen et al., 2001, 1994; Morley et al., 2018) but in outer hair cells (Elgoyhen and Katz, 2012; Goutman et al., 2015) and different immune cells (Peng et al., 2004), it is possible that the observed anti-inflammatory activity is mediated by inhibition of $\alpha 9\alpha 10$ AChRs expressed in lymphocytes. Since a direct correlation between depression and inflammation has also been shown (Christmas et al., 2011), it is plausible that the antidepressant (Varia and Rauscher, 2002) and anti-inflammatory (Sacre et al., 2010) effects of (±)-citalopram might be mediated, at least partially, by its inhibitory activity on $\alpha 9\alpha 10$ AChRs. However, the functional interaction of (±)-citalopram with $\alpha 9\alpha 10$ AChRs has not previously determined. Since this is a prerequisite to decipher this relationship, the activity of (±)-citalopram was studied on $\alpha 9\alpha 10$ AChRs expressed in *Xenopus* oocytes by voltage-clamp recordings and its mechanism of action determined by voltage-dependence, ligand competition, molecular docking, and *in silico* mutation experiments.

A better understanding of the functional interaction and selectivity of SSRIs for different AChR subtypes, especially $\alpha 3\beta 4$ and $\alpha 9\alpha 10$ AChRs, is crucial to develop novel analogs for safer pharmacotherapies.

2. Materials and methods

2.1. Material

[³H]Imipramine hydrochloride (47.5 Ci/mmol) was obtained from PerkinElmer Life Sciences Products, Inc. (Boston, MA) and stored at -20°C . (±)-Citalopram hydrobromide was purchased from MedChemExpress USA (New Jersey, USA). (±)-Epibatidine hydrochloride and QX-314 were obtained from Tocris Bioscience (Ellisville, MO, USA). Fluo-4 was obtained from Molecular Probes (Eugene, Oregon, USA). Euthasol (sodium pentobarbital, 100 mg/kg; sodium phenytoin, 12.82 mg/kg) was obtained from LeVet Pharma (Oudewater, Netherlands). Polyethylenimine, acetylcholine (ACh), probenecid, atropine, imipramine hydrochloride, and bovine serum albumin (BSA), were purchased from Sigma Chemical Co. (St. Louis, MO, USA). Salts were of analytical grade.

2.2. Ca^{2+} influx measurements in cells expressing $\text{ha}3\beta 4$, $\text{ha}4\beta 2$ or $\text{ha}7$ AChRs

Ca^{2+} influx measurements were performed on HEK293- $\text{ha}3\beta 4$, HEK293- $\text{ha}4\beta 2$, and GH3- $\text{ha}7$ cells as previously described (Arias et al., 2018a, 2018b, 2017, 2016, 2010a; 2010b, 2010c). Briefly, 5×10^4 cells per well were seeded 72 h prior to the experiment on black 96-well plates (Costar, New York, USA) and incubated at 37°C in a humidified atmosphere (5% CO_2 /95% air). Under these conditions, the majority of expressed $\text{ha}4\beta 2$ and $\text{ha}3\beta 4$ AChRs have the ($\alpha 4/3$)₃($\beta 2/4$)₂ stoichiometry (see Arias et al., 2016, and references therein). 16–24 h before the experiment, the medium was changed to 1% BSA in HEPES-buffered salt solution (HBSS) (130 mM NaCl, 5.4 mM KCl, 2 mM CaCl_2 , 0.8 mM MgSO_4 , 0.9 mM NaH_2PO_4 , 25 mM glucose, 20 mM Hepes, pH 7.4). On the day of the experiment, the medium was removed by flicking the plates and replaced with 100 μL HBSS/1% BSA containing 2 μM Fluo-4 and 2.5 mM probenecid. The cells were then incubated at 37°C in a humidified atmosphere (5% CO_2 /95% air) for 1 h.

To determine the antagonistic activity of (±)-citalopram (Fig. 1), plates were flicked to remove excess of Fluo-4, washed twice with HBSS/1% BSA, refilled with 100 μL of HBSS containing different concentrations of (±)-citalopram, and incubated for 5 min. Plates were finally placed in the cell plate stage of the fluorescent imaging plate reader (Molecular Devices, Sunnyvale, CA, USA), and 0.1 μM (±)-epibatidine was added from the agonist plate to the cell plate using the 96-tip pipettor simultaneously to fluorescence recordings for 3 min. A baseline consisting of 5 measurements of 0.4 s each was recorded. The laser excitation and emission wavelengths are 488 and 510 nm, at 1 W, and a CCD camera opening of 0.4 s.

2.3. Voltage clamp recordings on oocytes expressing $\text{ra}9\alpha 10$ AChRs

Rat $\alpha 9$ and $\alpha 10$ subunits were expressed in *Xenopus* oocytes as previously described (Ballesterio et al., 2005). Electrophysiological recordings were performed at -70 mV using two-electrode voltage-clamp (Arias et al., 2018b; Ballesterio et al., 2005). Oocytes were pre-incubated for 2 min with (±)-citalopram before adding acetylcholine (ACh) and (±)-citalopram. The average peak amplitude of three control ACh responses just before the exposure to (±)-citalopram was used to normalize the amplitude of each test response in the presence of the drug.

To further determine the mechanism of inhibition of (±)-citalopram, two approaches were used: (1) the EC_{50} values for ACh were obtained in the absence and presence of 8.0 μM (±)-citalopram (close to its experimental IC_{50} value; see Tables 1), and (2) current-voltage (I–V) relationships were obtained by applying 2-s voltage ramps from -120 to $+50$ mV, 10-s after the peak response to 10 μM ACh, in the presence and absence of 10 μM (±)-citalopram, from a holding

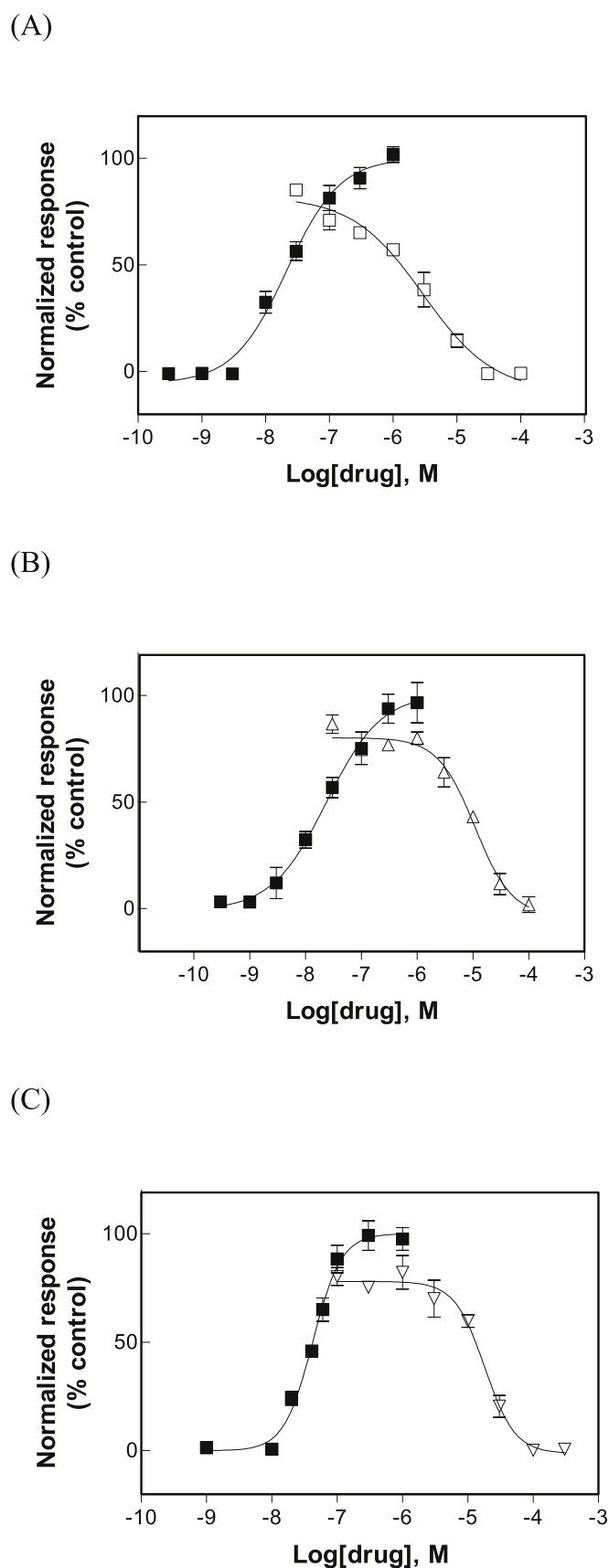


Fig. 1. Effect of (±)-citalopram on (±)-epibatidine-induced Ca²⁺ influx in HEK293-hα3β4 (A), HEK293-hα4β2 (B), and GH3-hα7 (C) cells. Increased concentrations of (±)-epibatidine (■) activated each hα3β4 (A), hα4β2 (B), and hα7 (C) AChR. Subsequently, cells were pre-treated (5 min) with several concentrations of (±)-citalopram (□), followed by addition of 0.1 μM (±)-epibatidine. Response was normalized to the maximal (±)-epibatidine response which was set as 100%. The plots are representative of 4–5 determinations, where the error bars are the S.D. The calculated IC₅₀ and n_H values are summarized in Table 1.

potential (V_{hold}) of -70 mV (Arias et al., 2018b). Leakage correction was performed by subtraction of the I–V curve obtained before the application of ACh.

2.4. Patch-clamp recordings on brain slices

An animal study protocol pertaining to this study (#IS00003604) was reviewed and approved by the Northwestern University Institutional Animal Care and Use Committee. Procedures also followed the guidelines for the care and use of animals provided by the National Institutes of Health (NIH) Office of Laboratory Animal Welfare. Mice were housed at 22 °C on a 12-h light/dark cycle with food and water *ad libitum*. Mice were weaned on postnatal day 21 and housed with same-sex littermates. Experiments were conducted on C57BL/6J mice obtained from Jackson Laboratories. All studies were restricted to male mice, age 8–24 weeks.

Brain slices were prepared as previously described (Arias et al., 2017; Shih et al., 2014). Mice were anesthetized with Euthazol (sodium pentobarbital, 100 mg/kg; sodium phenytoin, 12.82 mg/kg) before trans-cardiac perfusion with oxygenated (95% O₂/5% CO₂), 4 °C N-methyl-D-glucamine (NMDG)-based recovery solution that contains (in mM): 93 NMDG, 2.5 KCl, 1.2 NaH₂PO₄, 30 NaHCO₃, 20 HEPES, 25 glucose, 5 sodium ascorbate, 2 thiourea, 3 sodium pyruvate, 10 MgSO₄·7H₂O, and 0.5 CaCl₂·2H₂O; 300–310 mOsm; pH 7.3–7.4). Brains were immediately dissected after the perfusion and held in oxygenated, 4 °C recovery solution for 1 min before cutting a brain block containing the MHb and sectioning the brain with a vibratome (VT1200S; Leica). Coronal slices (250 μm) were sectioned through the medial habenula and transferred to oxygenated, 33 °C recovery solution for 12 min. Slices were then kept in holding solution (containing in mM): 92 NaCl, 2.5 KCl, 1.2 NaH₂PO₄, 30 NaHCO₃, 20 HEPES, 25 glucose, 5 sodium ascorbate, 2 thiourea, 3 sodium pyruvate, 2 MgSO₄·7H₂O, and 2 CaCl₂·2H₂O; 300–310 mOsm; pH 7.3–7.4) for 60 min or more before recordings.

Brain slices were transferred to a recording chamber being continuously superfused at a rate of 1.5–2.0 mL/min with oxygenated 32 °C recording solution. The recording solution contained (in mM): 124 NaCl, 2.5 KCl, 1.2 NaH₂PO₄, 24 NaHCO₃, 12.5 glucose, 2 MgSO₄·7H₂O, and 2 CaCl₂·2H₂O; 300–310 mOsm; pH 7.3–7.4). Patch pipettes were pulled from borosilicate glass capillary tubes (1B150F-4; World Precision Instruments, USA) using a programmable microelectrode puller (P-97; Sutter Instrument, USA). Tip resistance ranged from 4.5 to 8.0 MΩ when filled with internal solution. The following internal solution was used for the concentration-response experiments (in mM): 135 potassium gluconate, 5 EGTA, 0.5 CaCl₂, 2 MgCl₂, 10 HEPES, 2 MgATP, and 0.1 GTP; pH adjusted to 7.25 with Tris base. This internal solution also contained QX-314 (2 mM) for improved voltage control. The following internal solution was used for the voltage dependence experiments (in mM): 117 CsCH₃SO₃, 20 HEPES, 0.4 EGTA, 2.8 NaCl, 5 TEA-Cl, 2.5 MgATP, 0.1 spermine, and 0.25 MgGTP. The osmolarity of internal solutions were adjusted to 290 mOsm with sucrose.

Neurons within brain slices were visualized with infrared or visible differential interference contrast (DIC) optics. Neurons in the ventral inferior (VI) aspect of the MHb were targeted for recordings, as previously described (Arias et al., 2017; Shih et al., 2014). Electrophysiology experiments were conducted using a Scientifica SliceScope

Table 1
Inhibitory potency (IC₅₀) of (±)-citalopram at different AChR subtypes.

AChR subtype	Method	IC ₅₀ , μM	n _H ^f
hα3β4 ^a	(±)-Epibatidine-induced Ca ²⁺ influx in HEK293-hα3β4 cells	5.1 ± 1.3	1.00 ± 0.10
hα4β2 ^b	(±)-Epibatidine-induced Ca ²⁺ influx in HEK293-hα4β2 cells	19.0 ± 4.2	1.24 ± 0.19
hα7 ^c	(±)-Epibatidine-induced Ca ²⁺ influx in GH3-hα7 cells	18.8 ± 1.1	1.44 ± 0.22
α9α10 ^d	Voltage-clamp recordings of ACh-activated α9α10 AChRs expressed in <i>Xenopus</i> oocytes	7.5 ± 0.9	1.35 ± 0.10
Habenular mα3β4 ^{a,c}	Patch-clamp recordings of ACh-activated HMB (VI) neurons	7.6 ± 1.0	0.90 ± 0.10

^{a-e}Values were obtained from Figures.

^a 1A.

^b 1B.

^c 1C.

^d 2B, and.

^e 3B, respectively.

^f Hill coefficient.

Table 2
Potency of ACh (EC₅₀) in the absence and presence of (±)-citalopram at the α9α10 AChR.

ACh	EC ₅₀ (μM)	n _H
No (±)-citalopram	17.8 ± 1.8	0.98 ± 0.2
8.0 μM (±)-citalopram	134.6 ± 16.5	1.11 ± 0.6

Values obtained from Fig. 2B.

or Nikon FN-1 upright microscope. A computer running pCLAMP 10 software was used to acquire whole-cell recordings along with an Axopatch 200B amplifier and an A/D converter (Digidata 1440A). pClamp software and acquisition hardware were from Molecular Devices. Data were sampled at 10 kHz and low-pass filtered at 1 kHz. Immediately prior to gigaseal formation, the junction potential between the patch pipette and the superfusion medium was nulled. Series resistance was uncompensated.

To record physiological events following local application of drugs, a drug-filled pipette was moved to within 20–40 μm of the recorded neuron using a second micromanipulator. The drug (dissolved in recording solution) was dispensed onto the recorded neuron by using a Picopump (World Precision Instruments) at an ejection pressure of 12 psi for 250 ms. The ejection volume varied depending on the goal of the experiment. Atropine (1 μM) was present in the superfusion medium when using ACh application to prevent activation of muscarinic AChRs. To determine the voltage-dependence of (±)-citalopram-induced inhibition, voltage ramps (200 ms) were applied from the holding potential of –60 mV to a final value of 50 mV before returning to –60 mV. For such experiments, ACh was puff-applied and the ramp was executed during steady-state AChR currents. AChR-mediated currents were measured at both –60 mV and +50 mV in the same neuron before and after superfusion of (±)-citalopram (60 μM).

The voltage dependence of an inhibiting agent is related with the electrical distance of its binding site, measured from the external side of the membrane channel. Thus, the fraction of the electrical field sensed at the citalopram's binding site within the receptor's ion channel (i.e., δ), was subsequently calculated using the one-site blocking model (López-Valdés and García-Colunga, 2001):

$$(I_{ACh} / I_{ACh+Cit}) - 1 = [Citalopram] / IC_{50}(0) e^{(\delta z F V_m / RT)} \quad (1)$$

where, [Citalopram] is the concentration of the ligand, IC₅₀(0) is the ligand concentration to produce 50% inhibition at 0 mV, V_m is the applied membrane potential, z is the valence of the blocking molecule, F is the Faraday constant, R is the gas constant, and T is the absolute temperature.

2.5. [³H]Imipramine competition binding experiments using either hα3β4 or hα4β2 AChR-containing membranes

To determine whether (±)-citalopram binds to the imipramine sites at hα3β4 and hα4β2 AChRs, [³H]imipramine competition binding experiments were performed using either hα3β4 or hα4β2 AChR-containing membranes prepared from the respective HEK293-hα3β4 and HEK293-hα4β2 cells, as previously described (Arias et al., 2010a, 2010b; 2010c). In this regard, hα3β4 or hα4β2 AChR-containing membranes (1.5 mg/mL) were suspended in binding saline buffer (50 mM Tris–HCl, 120 mM NaCl, 5 mM KCl, 2 mM CaCl₂, 1 mM MgCl₂, pH 7.4) and pre-incubated with 15.2 nM [³H]imipramine in the presence of 0.1 μM (±)-epibatidine (receptors are mainly in the desensitized state) for 30 min at room temperature (RT). The total volume was divided into aliquots, and increasing concentrations of the ligand under study were added to each tube and incubated for 2 h at RT. The non-specific binding was determined in the presence of 100 μM imipramine.

AChR-bound [³H]imipramine was then separated from free ligand by a filtration assay using a 48-sample harvester system with GF/B Whatman filters (Brandel Inc., Gaithersburg, MD, USA), previously soaked with 0.5% polyethylenimine for 30 min. The membrane-containing filters were transferred to scintillation vials with 3 mL of Bio-Safe II (Research Product International Corp, Mount Prospect, IL, USA), and the radioactivity was determined using a Beckman 6500 scintillation counter (Beckman Coulter, Inc., Fullerton, CA, USA).

2.6. Analysis methods

The concentration–response results from heterologous cells and MHB neurons, as well as from the radioligand competition binding experiments were curve-fitted by nonlinear least squares analysis using the Prism software (GraphPad Software, San Diego, CA), and the respective EC₅₀, IC₅₀, and n_H values calculated. The obtained IC₅₀ values for (±)-citalopram were transformed into inhibition constants (K_i) using the Cheng–Prusoff relationship (Cheng and Prusoff, 1973):

$$K_i = IC_{50} / \{1 + ([^3H]imipramine) / K_d^{imipramine}\} \quad (2)$$

where [³H]imipramine is the initial concentration of [³H]imipramine, and K_d^{imipramine} is the dissociation constant for [³H]imipramine at the hα3β4 [0.41 μM (Arias et al., 2010c)] and hα4β2 [0.83 μM (Arias et al., 2010b)] AChRs.

The binding affinity and voltage-dependence differences were determined by Student's t-test analysis.

2.7. Molecular docking and molecular dynamics simulations

Since the functional experiments were performed with hα3β4 AChRs in the (α3)₃(β4)₂ stoichiometry (Arias et al., 2016), and (α9)₂(α10)₃ is the most probable form (Boffi et al., 2017; Plazas et al.,

2005), these two AChR stoichiometries were first built using the X-ray structure (PDB ID: 5KXI) of the human $\alpha 4\beta 2$ AChR at 3.9 Å resolution (Morales-Perez et al., 2016) as the homologous template using the MODELLER program (Šali et al., 1995) as implemented in the Accelrys Discovery Studio 2.5 software.

(+)-Citalopram in the protonated state (i.e., protonated at physiological pH) was modeled using VEGA ZZ and subsequently docked at each AChR model using AutoDock Vina (Trott and Olson, 2010). Protocols for minimization, partial charge calculations and docking were carried out as previously described (Arias et al., 2018a, 2018b, 2016).

To determine the stability of each pose within its predicted docking site, 20-ns molecular dynamics (MD) simulations were performed as previously described (Arias et al., 2018a, 2018b, 2016), using NAMD (Phillips et al., 2005) and CHARMM force field, and VEGA ZZ (Pedretti et al., 2004) as interface. Poses with RMSD variance (VAR) < 1 during the last third of the MD were used.

2.8. Calculation of the theoretical binding energies

Theoretical binding energies (TBE), measured from the individual poses at the end of the MD, were calculated using molecular mechanics as in (Arias et al., 2018a, 2018b). The TBE values are estimations used only for comparative purposes among receptors and its respective sites, and do not intend to represent absolute binding energies. More negative TBE values indicate higher theoretical binding affinities (TBA).

2.9. In silico mutations

To structurally explain the different binding behavior of escitalopram between $(\alpha 3)_3(\beta 4)_2$ and $(\alpha 9)_2(\alpha 10)_3$ models, *in silico* mutations were performed on those amino acid positions involved in orthosteric and luminal binding, respectively, using homologous residues from subunits $\alpha 3$, $\alpha 9$, or $\alpha 10$. Mutations were implemented using the Build Mutants module implemented in the Accelrys Discovery Studio 2.5 software which also use the MODELLER algorithms (Šali et al., 1995) for this purpose.

3. Results

3.1. AChR selectivity for (±)-citalopram

The activation potency of (±)-epibatidine on each human AChR was first determined by assessing the fluorescence change in the respective AChR-expressing cells after (±)-epibatidine stimulation. The respective EC₅₀ values for (±)-epibatidine are in the same range as previous determinations (Arias et al., 2018a, 2018b, 2017, 2016, 2010a; 2010b, 2010c).

The inhibitory activity of (±)-citalopram was subsequently assessed by pre-incubating (±)-citalopram with the respective $\alpha 3\beta 4$ (Fig. 1A), $\alpha 4\beta 2$ (Fig. 1B), and $\alpha 7$ -expressing cells (Fig. 1C), for 5 min before (±)-epibatidine stimulation (0.1 μM). Interestingly, (±)-citalopram inhibited (±)-epibatidine-induced $\alpha 3\beta 4$ AChR activity (IC₅₀ = 5.1 ± 1.3 μM) with higher potency compared to that for the $\alpha 4\beta 2$ (19.1 ± 1.3 μM) and $\alpha 7$ (18.8 ± 1.3 μM) AChRs (Table 1). The results showing that the n_H values for (±)-citalopram are near unity (Table 1) indicate that the inhibitory process is mediated by a non-cooperative mechanism. A non-cooperative mechanism, in turn, suggests that there is potentially only one binding site or several sites with similar affinity.

3.2. (±)-Citalopram inhibits $\alpha 9\alpha 10$ AChRs in a concentration-dependent and voltage-independent manner

Voltage-clamp experiments showed that (±)-citalopram inhibits ACh (10 μM)-evoked $\alpha 9\alpha 10$ AChR activity in a concentration-dependent manner (Fig. 2A and B), giving an IC₅₀ value of 7.5 ± 0.9 μM

(Table 1). The observed n_H value close to unity (Table 1) indicated that the inhibitory process is mediated by a non-cooperative mechanism. To further study the inhibitory mechanism elicited by (±)-citalopram, two approaches were used. First, the activity elicited by increasing concentrations of ACh was determined in the absence and presence of 8.0 μM (±)-citalopram (Fig. 2B). The competition curves showed that (±)-citalopram produced a parallel rightward shift of ACh-evoked responses. A significant (p = 0.0001) increase of the ACh EC₅₀ value (7.5-fold) was observed in the presence of (±)-citalopram, with no changes in agonist maximal responses and n_H values (Table 2), supporting a competitive mechanism of inhibition. Secondly, the inhibitory activity of 10 μM (±)-citalopram was determined at different membrane potentials, as shown in the representative I/V curve (Fig. 2C). The ACh responses were inhibited by (±)-citalopram at both negative (−90 mV) and positive (+40 mV) potentials with similar percentage (46.0 ± 4.7% and 43.3 ± 4.9%, respectively; Student's t-test; p = 0.1) (Fig. 2D), indicating that the observed inhibition is mainly voltage-independent and consistent with a competitive mode of action.

3.3. (±)-Citalopram inhibits ACh-evoked currents from MHb (VI) neurons in a concentration- and voltage-dependent manner

Patch-clamp recordings on MHb (VI) neurons showed that 100 μM ACh puffs activated endogenous AChRs (see control traces in Fig. 3A). MHb (VI) neurons were identified primarily by their close proximity (< 50–70 μm) to the 3rd ventricle within the ventral aspect of the MHb. They were secondarily distinguished from other nearby brain areas (e.g., thalamus and lateral habenula) via the presence of slow (1–8 Hz) tonic firing (Shih et al., 2014).

The observed inward currents elicited by ACh were reduced by superfusion of 60 μM (±)-citalopram (Fig. 3A), and drug washout resulted in complete recovery of the original response amplitude. Full recovery after washout confirms that the recording remained stable during drug applications. A concentration-dependent inhibition was determined for (±)-citalopram (Fig. 3B) by using a wide range of concentrations (i.e., 0.07–180 μM), giving an inhibitory potency of 7.6 ± 1.0 μM (Table 1). The observed n_H value close to unity (Table 1) suggested a non-cooperative mechanism.

To further examine the antagonistic mechanism of (±)-citalopram on native MHb AChRs, the inhibitory activity of this drug was compared at a holding potential of −60 mV and +50 mV in the same cell. (±)-Citalopram (60 μM) inhibited ACh-evoked responses by 42 ± 6% at negative potential (−60 mV; paired Student's t-test: p = 0.0002), whereas its effect at positive potential (+50 mV) was not statistically significant (84 ± 12%; p = 0.2536) compared with the values for ACh alone (Fig. 3C). Nevertheless, a significant difference was observed between these two extreme potentials (p = 0.0088). These results suggest that (±)-citalopram preferentially blocks habenular $\alpha 3\beta 4^*$ AChRs in a voltage-dependent fashion.

Considering that (±)-citalopram's activity is voltage-dependent, the electrical distance (δ) of its binding site along the ion channel, was subsequently calculated using Eq. (1). The determined IC₅₀(0) (92 μM) and δ (0.40) values suggested that citalopram isomers interact with a binding site located within the pore, close to the middle region of the ion channel.

3.4. Binding affinity of (±)-citalopram for the [³H]imipramine sites at either $\alpha 3\beta 4$ or $\alpha 4\beta 2$ AChRs

To determine whether (±)-citalopram binds to the [³H]imipramine at either $\alpha 3\beta 4$ or $\alpha 4\beta 2$ AChRs, the effect of this antidepressant on [³H]imipramine binding was determined on desensitized AChRs [i.e., in the presence of (±)-epibatidine] (Fig. 4). The results indicated that the binding affinity of (±)-citalopram for $\alpha 3\beta 4$ AChRs (K_i = 1.8 ± 0.1 μM) was > 2-fold higher than that for $\alpha 4\beta 2$ AChRs (4.1 ± 0.3 μM) (paired Student's t-test, p = 0.0009) (Table 3). Since

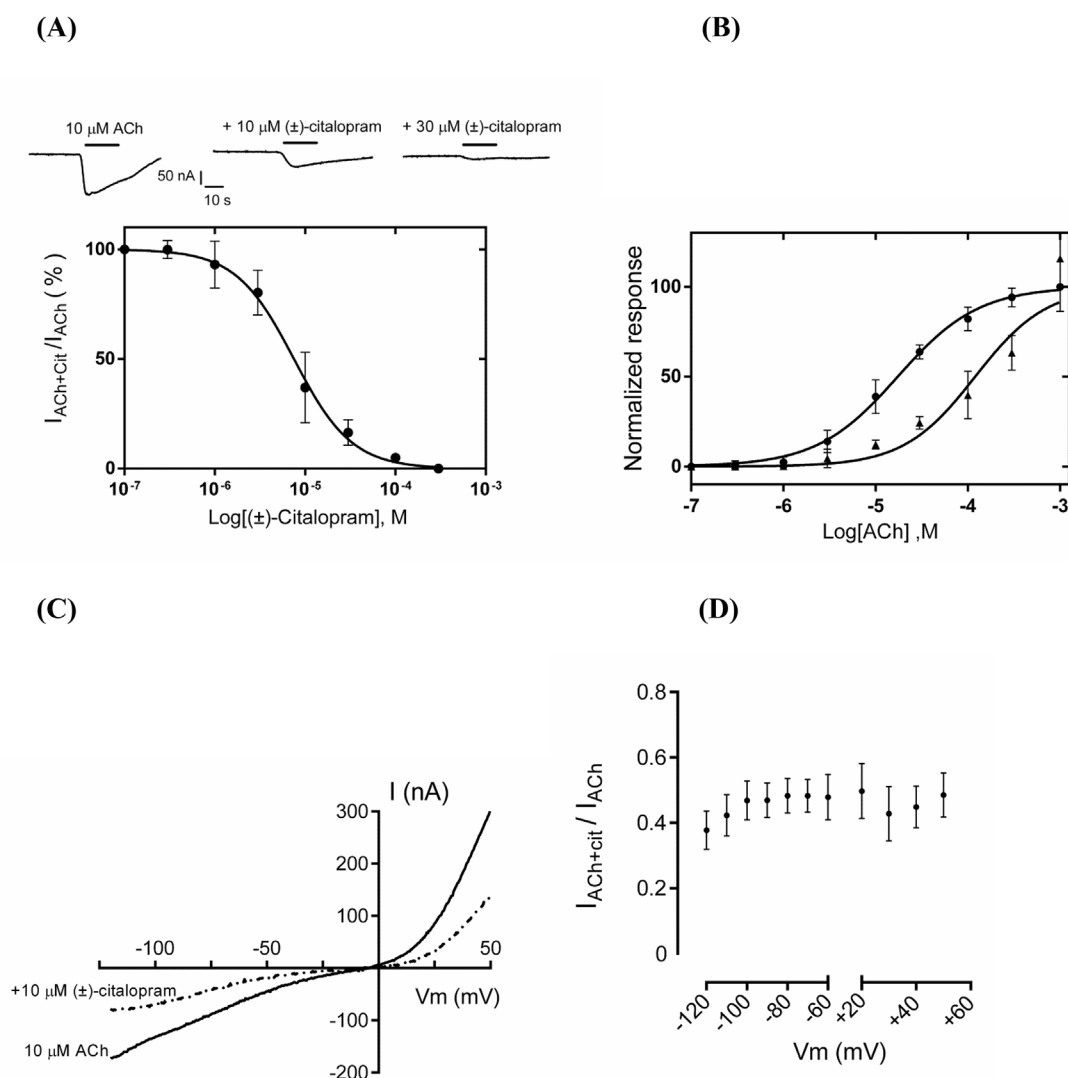


Fig. 2. Effect of (±)-citalopram on acetylcholine (ACh)-evoked activity at $\alpha 9\alpha 10$ AChRs expressed in *Xenopus* oocytes. (A) Responses of $\alpha 9\alpha 10$ AChRs elicited by 10 μ M ACh are diminished by increasing concentrations of (±)-citalopram. The inhibition curve was obtained by the co-application of 10 μ M ACh and increasing concentrations of (±)-citalopram ($r^2 = 0.96$; $n = 7$). Responses (mean \pm SEM) were normalized to that elicited by 10 μ M ACh (its EC_{50} value) which was set as 100%. The calculated IC_{50} and n_H values are summarized in Table 1 (B) Concentration-response curves for ACh in the absence (●) and presence (▲) of 8 μ M (±)-citalopram ($n = 6$). The EC_{50} values for ACh in the absence and presence of (±)-citalopram are summarized in Table 2. A statistical difference was obtained ($p = 0.0001$). (C) A representative current-voltage response ($n = 7$) obtained by applying 2-s voltage ramps from -120 to $+50$ mV, 10-s after the peak response to 10 μ M ACh from a holding potential (V_{hold}) of -70 mV, in the presence and absence of 10 μ M (±)-citalopram. (D) The comparison of (±)-citalopram-induced inhibition at different membrane potentials showed no statistical difference (Student's t-test; $p = 0.1$), indicating a voltage-independent mechanism ($n = 7$).

the binding affinity for resting $\alpha 4\beta 2$ AChRs [i.e., in the presence of 0.1 μ M κ -bungarotoxin (Arias et al., 2010a, 2010b; 2010c);] ($5.9 \pm 0.4 \mu$ M) was in the same range as that in the desensitized state, no additional experiments were performed on resting $\alpha 3\beta 4$ AChRs.

The observed n_H values (i.e., close to unity) (Table 3) indicated that (±)-citalopram inhibits [3 H]imipramine binding to either $\alpha 3\beta 4$ or $\alpha 4\beta 2$ AChR by non-cooperative mechanisms. This suggests, in turn, that there is potentially only one binding site or several sites with similar binding affinity on each AChR subtype.

3.5. Molecular docking and molecular dynamics simulations of S-(+)-citalopram (escitalopram) to the $h(\alpha 3)_3(\beta 4)_2$ and $h(\alpha 9)_2(\alpha 10)_3$ AChRs

In the $h(\alpha 3)_3(\beta 4)_2$ AChR model, two luminal sites for escitalopram were found by molecular docking (Fig. 5A), and their stability confirmed by molecular dynamics (Table 4; Fig. 5D). The docking procedure did not find any conformer at the orthosteric sites, but two non-

orthosteric sites (not shown for simplicity), which presumably do not directly influence nicotine binding.

The high-affinity binding site (TBE = -14.31 kcal/mol; Table 4) is located between positions 5' and 16', in the middle of the ion channel but toward the extracellular ion channel's mouth (Fig. 5A–E). The M2 residues at each position are: $\alpha 3$ -I246 (5'), $\beta 4$ -S248 (6'; Ser ring), $\alpha 3$ -L249 (8'), $\alpha 3$ -L250 and $\beta 4$ -L251 (9'; Leu ring), $\alpha 3$ -S251 and $\beta 4$ -A252 (10'), $\alpha 3$ -T253 and $\beta 4$ -T254 (12'); $\alpha 3$ -V254 and $\beta 4$ -F255 (13'; Val ring); $\alpha 3$ -F255 and $\beta 4$ -F256 (14'), and $\beta 4$ -L258 (16'). Favoring its higher affinity is the presence of a strong H-bond with the $\beta 4$ -T254 side chain oxygen. In addition, a cation- π interaction is established between the N^+ atom of escitalopram and the aromatic moiety of $\alpha 3$ -F255. The low-affinity binding site is located closer to the cytoplasmic side, between positions -3' and 6' (Table 4). The M2 residues at each position are: $\alpha 3$ -G239 and $\beta 4$ -G240 (-3'; Gly ring), $\alpha 3$ -E240 and $\beta 4$ -E241 (-2'), $\alpha 3$ -V242 and $\beta 4$ -M243 (1'), $\alpha 3$ -T243 and $\beta 4$ -T244 (2'; Thr ring), $\beta 4$ -L245 (3'), $\alpha 3$ -I246 and $\beta 4$ -I247 (5'), and $\alpha 3$ -S247 and $\beta 4$ -S248 (6'). No H-bond nor cation- π interactions were detected at this site. Residues

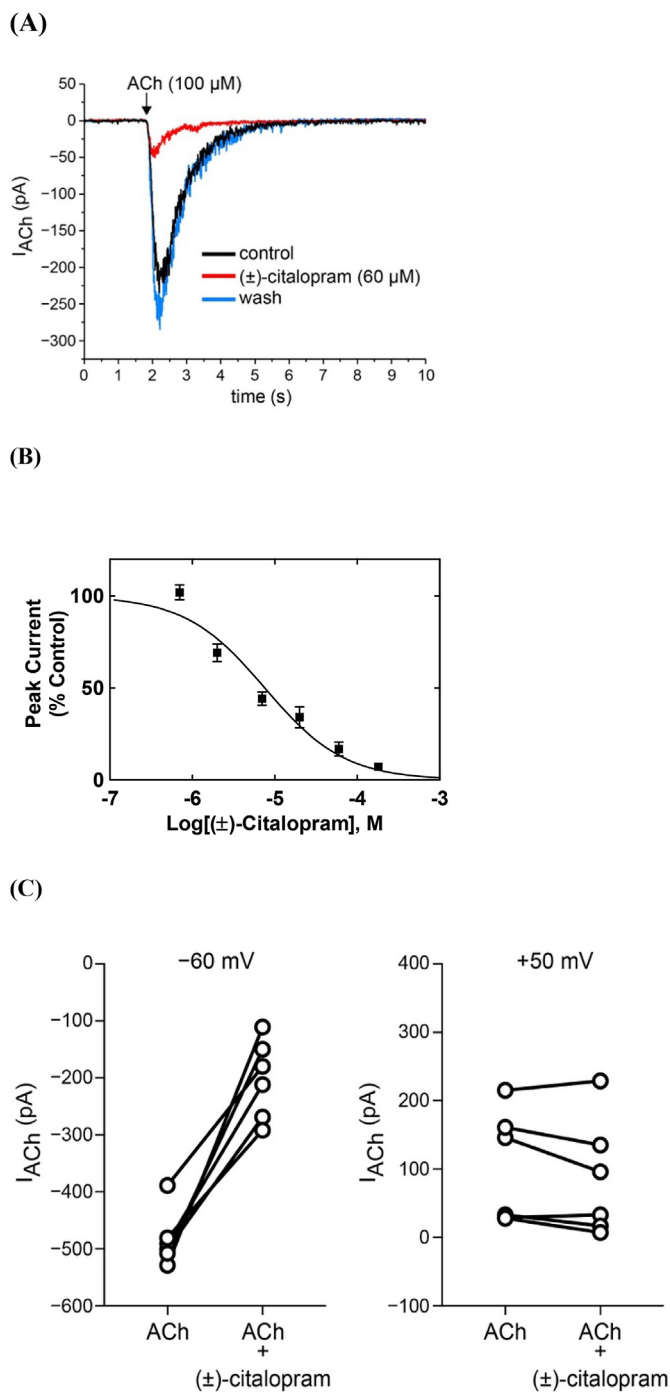


Fig. 3. Inhibitory potency of (\pm)-citalopram on ACh-evoked currents from MHb (VI) neurons. (A) ACh puff (100 μ M)-evoked currents from MHb (VI) neurons are decreased by 60 μ M (\pm)-citalopram. The puff was performed for 250 ms at a pressure of 12 psi. After washing, the peak amplitude completely recovered, indicating a reversible inhibition. (B) Concentration-response relationship for the inhibitory activity of (\pm)-citalopram on ACh-evoked currents from MHb (VI) neurons. Response was normalized to the maximal ACh response which was set as 100%. The plot ($r^2 = 0.90$) is representative of 5–8 determinations (mean \pm SEM). The calculated IC_{50} and n_H values are summarized in Table 1 (C) Voltage-dependence of (\pm)-citalopram-induced inhibition of ACh-evoked currents from MHb (VI) neurons. Steady-state ACh puff (100 μ M)-evoked currents from MHb (VI) neurons were recorded at -60 mV and +50 mV in the same cell, in the absence and presence of 60 μ M (\pm)-citalopram. Data plots show ACh-activated currents before and after (\pm)-citalopram superfusion at the indicated membrane potential. Paired Student's t-test analyses indicated that (\pm)-citalopram reduced ACh-evoked response amplitudes by $42.4 \pm 6.1\%$ at -60 mV ($p = 0.0006$) and $74.6 \pm 13.6\%$ at +50 mV ($p = 0.1494$).

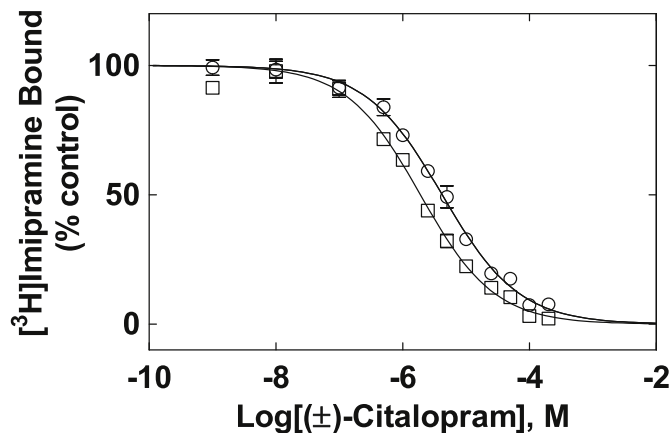


Figure 4. (\pm)-Citalopram-induced inhibition of [3 H]imipramine binding to either $\alpha 3\beta 4$ (\square) or $\alpha 4\beta 2$ (\circ) AChRs in the desensitized state. Each AChR-containing membrane (1.5 mg/mL) was pre-incubated (30 min) with 15.2 nM [3 H]imipramine in the presence of 0.1 μ M (\pm)-epibatidine (receptors are mainly in the desensitized state), and then equilibrated with increasing concentrations of (\pm)-citalopram. Nonspecific binding was determined at 100 μ M imipramine. The plots are combinations of 2–4 experiments, each performed in triplicate, where the error bars are the S.D. The IC_{50} and n_H values were obtained by nonlinear least-squares fit of the plots ($r^2 = 0.95$ for both). The K_i values, calculated using Eq. (1), were summarized in Table 2.

Table 3

Binding affinity of (\pm)-citalopram for the [3 H]imipramine sites at the respective $\alpha 3\beta 4$ and $\alpha 4\beta 2$ AChRs in the desensitized state.

AChR subtype	K_i , μ M ^a	n_H ^b
$\alpha 3\beta 4$	1.8 ± 0.1	0.74 ± 0.04
$\alpha 4\beta 2$	4.1 ± 0.3	0.72 ± 0.03

^a The IC_{50} values obtained from Fig. 4 were transformed into K_i values using Eq. (2).

^b Hill coefficient.

$\alpha 3$ -I246 (5') and $\beta 4$ -S248 (6') from this site belong to different subunit copies respect to those belonging to the high-affinity site at the pentameric $h(\alpha 3)_3(\beta 4)_2$ receptor.

In the $h(\alpha 9)_2(\alpha 10)_3$ model, escitalopram interacted with three orthosteric binding sites (Fig. 6A) located in the interface between (+) $\alpha 10$ (principal component) and (-) $\alpha 9$ or another (-) $\alpha 10$ (complementary component) (Boffi et al., 2017). Their stabilities were confirmed by molecular dynamics (Fig. 6D; Table 5). The conformers at sites 1 and 2 found at the (+) $\alpha 10$ /(-) $\alpha 9$ interface showed higher TBA values than that for site 3 (Table 5). Several additional docking sites were found but none of them positioned in such a way to sterically block the ion channel (i.e., at or near the middle of the channel). Moreover, no conformers were found at the non-orthosteric binding sites [i.e., (-) $\alpha 10$ /(+) $\alpha 9$].

The three sites have residues coming from the same receptor domains. The complementary component [(-) $\alpha 9$] is formed by six common residue positions from the $\beta 1$, $\beta 2$, $\beta 3$, $\beta 5$ and $\beta 6$ sheets. Four of them coincide with those for (-)-nicotine binding (i.e., canonical positions) (Brejc et al., 2001), including R59 ($\beta 2$ sheet), V111 ($\beta 5$ sheet), $\alpha 9$ -T119- $\alpha 10$ -R119 and D121 ($\beta 6$ sheet) (Table 5), and two novel positions at $\alpha 9$ -Q36- $\alpha 10$ -E36 and V111. Sites 1 and 2 have two common positions, W57 (a canonical site), and W120. Other residues involved are (-) $\alpha 10$ -T34 (site 3), N60, S79, and the canonical R113 (site 2). Eleven common residues, coming only from the (+) $\alpha 10$ subunit, form the principal component. Five of them agree with canonical (-)-nicotine binding positions (Brejc et al., 2001), including Y95 ($\beta 4$ - $\beta 5$ loop), W151 ($\beta 7$ - $\beta 8$ loop), C194-C195 ($\beta 9$ - $\beta 10$ loop), and Y199 ($\beta 10$ sheet) (Table 5). Other common residues include S150, G154,

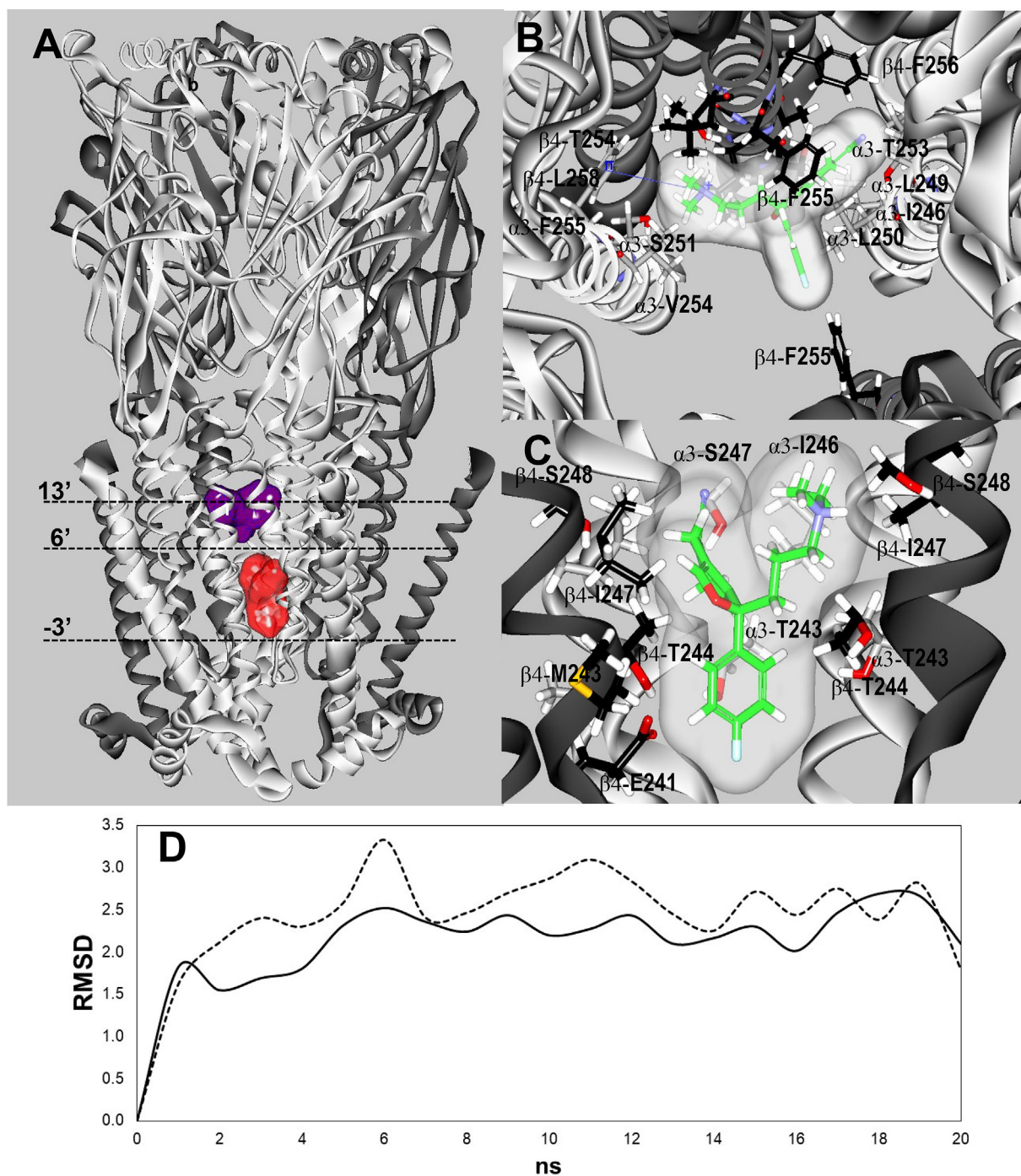


Fig. 5. (A) Docking sites for S-(+)-citalopram (escitalopram) at the h(α 3) $_3$ (β 4) $_2$ AChR model. Escitalopram docked to two luminal sites (surface model), a high-affinity site located closer to the extracellular ion channel's mouth (blue) and a low-affinity site located closer to the cytoplasmic side (red). α 3 (white) and β 4 (dark grey) subunits are represented as solid ribbons. Dotted lines indicate the positions of Gly (position -3'), Ser (position 6'), and Val (position 13') rings along the ion channel. (B) In the high-affinity site, escitalopram (as sticks and its transparent surface model, colored by atoms with carbons in green) interacted with M2 residues located between positions 5' and 16', forming a strong H-bond with β 4-T254 (position 12') (dotted black line), and a cation- π interaction with α 3-F255 (position 14') (solid blue line). (C) In the low-affinity site, escitalopram interacted with M2 residues located between positions -3' and 6'. A complete list of residues is summarized in Table 4. The interacting residues (as sticks) are labeled by their subunit, residue one letter code, and amino acid sequence number, and colored by atoms, including carbons (grey for the α 3 subunit, and black for the β 4 subunit), nitrogens (blue), oxygens (red), and hydrogen (white). (D) Molecular dynamics simulations (20 ns) of escitalopram interacting with the high- (---) and low-affinity (—) sites, respectively, at the h(α 3) $_3$ (β 4) $_2$ model.

Y192, G193, S196, and E197. In addition, T152 is shared by sites 2 and 3.

At site 1, α 10-C194 establishes a H-bond between its main chain O and a H of one of the methyl groups attached to the ammonium moiety of escitalopram (Fig. 6B), whereas another H-bond is formed between the E197 side chain O and a H of the phenyl group. At this site,

escitalopram has a conformation that enables it to establish an intramolecular cation- π interaction between N $^+$ and the fluorophenyl ring. At site 2, two H-bonds are formed, one between escitalopram's fluorine and the H of the α 9-T119 side chain, and another between escitalopram's ammonium H and the hydroxyl O of the α 9-D121 side chain. In addition, there is a network of cation- π interactions: the

Table 4
Residues involved in the docking of S-(+)-citalopram (escitalopram) to luminal sites at the h(α 3)₃(β 4)₂ AChR.

Luminal Site	TBE (Kcal/mol)	RMSD Mean/Var	α 3	β 4	Homologous residues ^a		M2 Position (ring)
					α 9	α 10	
High- affinity	− 14.31	2.30/0.02	I246*		V248	V248	5'
				S248*	T249	T249	6' (Ser)
			L249		L251	L251	8'
			L250	L251	L252	L252	9' (Leu)
			S251	A252	A253	A253	10'
			T253	T254 (H-bond donor)	T255	T255	12'
			V254	F255	V256	V256	13' (Val)
			F255 (Cation- π)	F256	F257	F257	14'
				L258	L259	L259	16'
				G239	G241	G241	− 3' (Gly)
Low- affinity	− 4.27	2.55/0.07	E240	G240	E242	E242	− 2'
			V242	M243	V244	V244	1'
			T243	T244	S245	S245	2' (Thr)
				L245	L246	L246	3'
			I246*	I247	V248	V248	5'
			S247	S248*	T249	T249	6' (Ser)

*Residues from the high- and low-affinity sites belong to different α 3 and β 4 subunit copies, indicating no overlapping between both sites.

^a The homologous residues at α 9 and α 10 subunits are also included for comparative purposes.

intramolecular interaction also seen at site 1 for escitalopram, and the intermolecular interaction between the N⁺ of escitalopram and both rings of α 10-W151 and the phenyl ring of α 10-Y199 (Fig. 7). Finally, site 3 is the only one composed by two adjacent α 10 subunits. At this site, escitalopram establishes a cation- π interaction with R119 and a H-bond between the O of the α 10-G193 main chain and the ammonium H of escitalopram.

3.6. Structural differences between escitalopram docked to the h(α 3)₃(β 4)₂ and h(α 9)₂(α 10)₃ AChRs

Considering that both h(α 3)₃(β 4)₂ and h(α 9)₂(α 10)₃ AChR models are based on the same template, differences in docking results must be due to, and should be explained by alterations in the amino acid sequences as follow.

3.6.1. Luminal sites

Two luminal sites for escitalopram were characterized at the h(α 3)₃(β 4)₂ but none was observed at the h(α 9)₂(α 10)₃ (Fig. 5). To find out the structural reasons of this difference at the amino acid level, a comparison was made between homologous M2 residues involved in escitalopram binding at both receptors (Table 4). Both receptors have the same amino acids at positions 8', 9', 12', 14', and 16', where the high-affinity site for escitalopram is located. However, I246 (position 5') is only found at α 3, whereas V248, the homologous residue at α 9 and α 10, is also hydrophobic but slightly smaller. At ring 6', β 4-S248 is substituted by the slightly larger but also polar residue T249 in α 9 and α 10. Although these differences may have some influence on escitalopram binding, there is a more important modification at position 10' between the polar α 3-S251 and its homologous residue, the hydrophobic α 9-A253 (both β 4 and α 10 have Ala at this position). The key difference between both receptors is centered on ring 13', where β 4 has a Phe residue (F255), while all other subunits have Val. Fig. 5B shows that F255 protrudes to the middle of the ion channel from one side making a direct contact with escitalopram docked at the opposite side, supporting a total blockage of the lumen. This interaction is structurally not possible at the h(α 9)₂(α 10)₃ AChR, since the homologous residue, V254, is smaller and does not contact escitalopram.

In the low-affinity site, escitalopram is stacked at the cytoplasmic and narrowest end of the h(α 3)₃(β 4)₂ channel. There are three M2 sequence differences between both receptors: at position 1', β 4 has a Met residue (M243), whilst the other subunits have Val as the homologous residue. However, since the larger side chain of M243 is not

facing the lumen, it has no influence on ligand binding (Fig. 5C). There are two important differences between both receptors. One is at ring 2', where a larger Thr residue is present in h(α 3)₃(β 4)₂ (Fig. 5C) compared to Ser at h(α 9)₂(α 10)₃ (Table 4). The other is at ring 5', where h(α 3)₃(β 4)₂ has a larger Ile residue compared to a Val present at h(α 9)₂(α 10)₃.

To determine the importance of these structural differences, receptor mutants were constructed, and escitalopram docked as described previously. The h(α 3)₃(β 4)₂ mutations included β 4F255V (to test the high-affinity luminal site), and α 3T243S, α 3I246V, β 4T244S, β 4I244V (to test the low-affinity luminal site). The h(α 9)₂(α 10)₃ mutations included α 9V256F (high-affinity site), and α 9 α 10S245T and α 9 α 10V248I (low-affinity site). The h(α 3)₃(β 4)₂ mutations abolished the docking of escitalopram at both luminal sites. When h(α 9)₂(α 10)₃ carried only the α 9V256F mutation, escitalopram was able to dock to a locus similar to the high-affinity, and when the remaining α 9 α 10S245T and α 9 α 10V248I mutations were added, escitalopram could also dock to a locus similar to the low-affinity site.

3.6.2. Orthosteric binding sites

Our *in silico* studies indicated that escitalopram docked at the orthosteric binding sites of the h(α 9)₂(α 10)₃ (Fig. 6), but not h(α 3)₃(β 4)₂ AChRs. In addition, escitalopram docked to non-orthosteric binding sites at the latter receptor but not to the former. Escitalopram does not bind to “non-orthosteric” sites in the h(α 9)₂(α 10)₃ AChR because the (+) α 9 side is not capable of behaving as does (+) α 10, even considering that it has the characteristic adjacent double Cys residues at the binding site.

In order to explain why escitalopram does not bind to h(α 3)₃(β 4)₂ orthosteric sites, we compared the amino acid sequence between the (+) sides of α 3 and α 10, the (−) sides of α 9 or α 10 [since the latter is also able to behave as a (−) side in site 3] and β 4, or both types of differences (Table 5). For the (+) side, a comparison with (+) α 9 residues is also shown.

Essential positions, useful for comparison analysis, are those that are common to the three sites at the h(α 9)₂(α 10)₃. There are seven such positions at the (−) side, none of which can explain the absence of binding at h(α 3)₃(β 4)₂. More specifically: (1) Same homologous residues [e.g., α 9-Q36 and β 4-Q38 (1st position), α 10-E61 and β 4-E63 (3rd position), and Arg in all subunits (4th position)]; (2) Structurally similar homologous residues that maintain the same basic functions [e.g., charged α 9-and α 10-R59 vs β 4-K61 (2nd position), hydrophobic α 9-and α 10-V111 vs β 4-I113 (5th position)]; (3) Different homologous

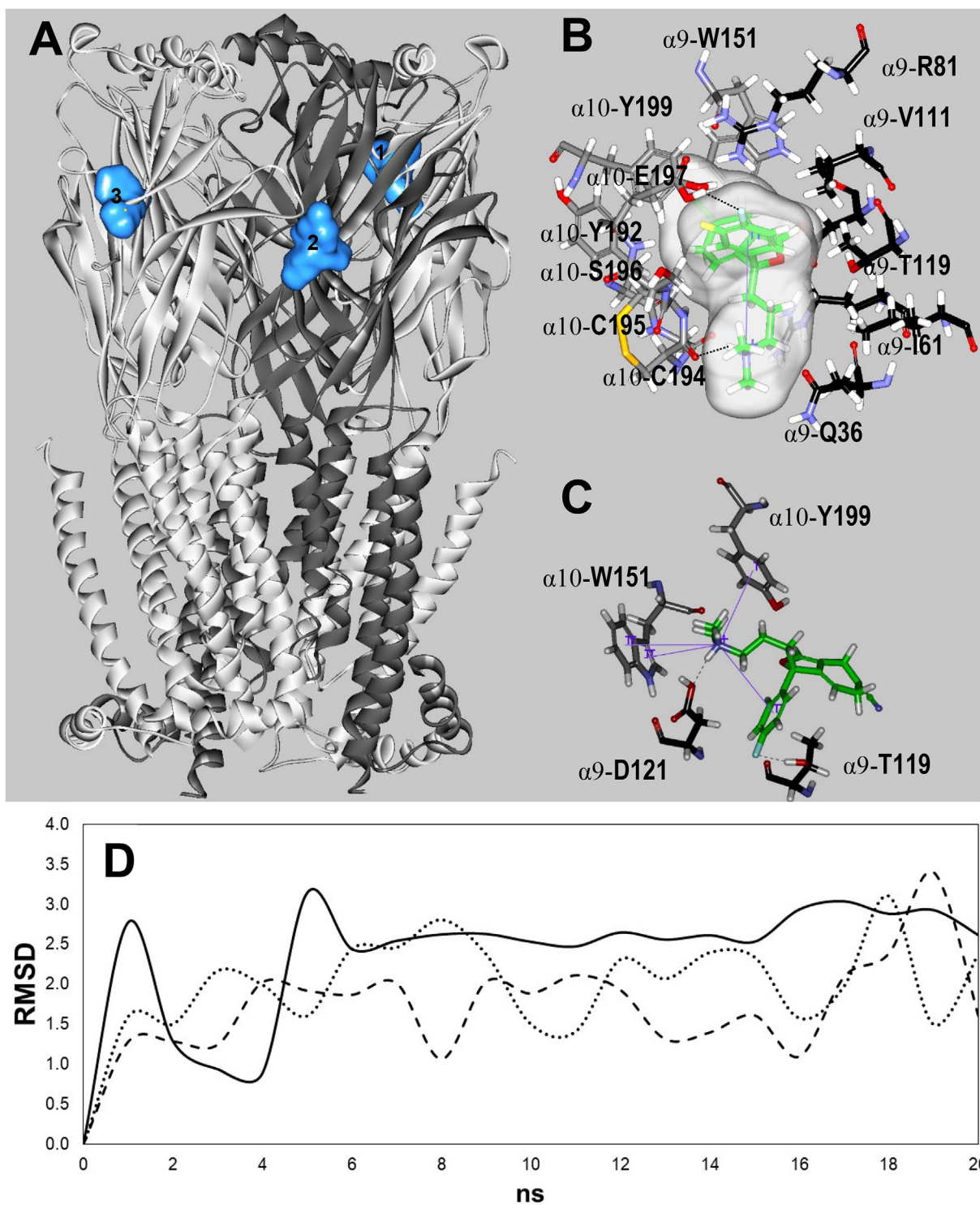


Fig. 6. Docking sites for S-(+)-citalopram (escitalopram) at the h($\alpha 9$)₂($\alpha 10$)₃ AChR model. (A) Escitalopram interacted with three possible orthosteric sites located at the interface between the (+) $\alpha 10$ (principal component) and ($-$) $\alpha 9$ [or another ($-$) $\alpha 10$] subunit (complementary component) (light blue surface models). $\alpha 10$ (white) and $\alpha 9$ (dark grey) subunits are represented as solid ribbons. (B) In site 1, escitalopram (as sticks and its transparent surface model, colored by atoms with carbons in green) formed a strong H-bond with two oxygens, one on the $\alpha 10$ -C194 main chain and another on the $\alpha 10$ -E197 side chain (dotted black line). Interestingly, an intramolecular cation- π interaction is formed in escitalopram, between N^+ and its fluorophenyl ring (solid blue line). (C) In site 2, escitalopram (as sticks colored by atoms with carbons in green) formed a network of H-bond and cation- π interactions. Other details are included in Fig. 5. The complete list of residues interacting at each site is summarized in Table 5 (D) Molecular dynamics simulations (20 ns) of escitalopram interacting with sites 1 (—), 2 (---), and 3 (.....), respectively, at the h($\alpha 9$)₂($\alpha 10$)₃ model.

Table 5Residues involved in the docking of S-(+)-citalopram (escitalopram) to the agonist binding sites at the h(α 9)₂(α 10)₃ AChR.

Orthosteric Site	1	2	3	
TBE (Kcal/mol)	-15.22	-14.85	-12.13	
RMSD (Mean/Var)	1.75/0.14	2.58/0.019	2.34/0.15	Homologous residues ^a
Secondary Structure	Subunit and Residues			
β 1 Sheet	(-) α 9	(-) α 9	(-) α 10	(-) β 4
	Q36	Q36	T34	Q38
β 2 Sheet	W57(-)	W57(-)	R59(-)	K61
	R59(-)	R59(-)	R59(-)	
	N60			
β 3 Sheet	I61	I61	E61	E63
		S79		
β 5 Sheet	R81	R81	R81	R83
	V111(-)	V111(-)	V111(-)	I113
β 6 Sheet	T119(-)	T119(-)	R119(-)	L121
	W120	W120		
	D121(-)	D121(-)	D121(-)	L123
	(+) α 10	(+) α 10	(+) α 10	(+) α 9
β 4- β 5 Loop	Y95(+)	Y95(+)	Y95(+)	(+) α 3
β 7 Sheet	S150	S150	S150	Y95
β 7- β 8 Loop	W151(+)	W151(+)	W151(+)	S148
		T152		W149
β 9- β 10 loop	G154	G154	G154	N154
	Y192	Y192	Y192	D152
	G193	G193	G193	Y190
	C194(+)	C194(+)	C194(+)	N191
	C195(+)	C195(+)	C195(+)	C192
	S196	S196	S196	C193
	E197	E197	E197	E194
β 10 Sheet	Y199(+)	Y199(+)	Y199(+)	E195
				Y197

Bold: residues forming H-bonds; *Italics:* residues forming cation- π interactions. Principal (+) or complementary (-) canonical component.

^a The homologous residues at α 3 and β 4 subunits are also included for comparative purposes.

residues where neither charge nor steric hindrance play an important role [e.g., polar α 9-T119 is not involved in H-bonding, and charged α 10-R119 is similarly bulky as the hydrophobic residue β 4-L121 at site 1 (6th position)]; (4) Although there is a difference between α 9-/ α 10-D121 and β 4-L123 (7th position), Asp is involved in H-bonding only at site 2, so polarity is not essential and both type of residues are similar in size.

At the (+) side there are twelve positions, eleven of which have the same residue at the α 9 and α 10 subunits (Table 5). There is only one position where both α 9 and α 3 subunits differ from α 10. The homologous residues of α 10-G154 are α 9-N154 and α 3-D152, respectively. α 3 also differs from α 10 at α 10-G193, where the former has an Asn191 residue, and at α 10-S196, where α 3 has a Glu194 residue (Table 5). To test if these residues are the basis of escitalopram binding at the orthosteric sites, *in silico* mutants were constructed and molecular docking performed as previously explained. The mutations α 3D152G, α 3N191G, and α 3E194S did not enable escitalopram binding to h(α 3)₃(β 4)₂. Likewise, the mutation α 9N194G did not enable escitalopram binding to (+) α 9. Conversely, the mutations α 10G154D, α 10G193N, or α 10S196E, which we expected should be important because they could promote an overlapping with escitalopram (Fig. 7), did not abolish escitalopram binding to h(α 9)₂(α 10)₃. Therefore, other structural reasons must be responsible for the preference of escitalopram binding to the orthosteric sites at h(α 9)₂(α 10)₃ but not at h(α 3)₃(β 4)₂ receptors. Consequently, we visually inspected the superposed α 3, α 9, and α 10 orthosteric binding sites with escitalopram docked at (+) α 10 (Fig. 8A and B). We found that the β 9- β 10 loop, which contains the Cys pair typical of α subunits, was widely open in α 10 allowing escitalopram to fit into the binding site. This loop is closer to the receptor center in α 9, and it is even closer in α 3, and causes

escitalopram to overlap the main chain atoms of these subunits when is at the (+) α 10 docking position. During model construction, loops are optimized according to the surrounding residues. Fig. 8C shows a sequence comparison of the surrounding residues. We found at least two possible residues (in blue) that could force the β 9- β 10 loop in α 10 to set apart from the receptor. From the β 9 sheet (Fig. 8D), α 10R186, which points to the middle of the β 9- β 10 loop and is bulkier than α 9V186 and α 3Y184, and from the β 10 sheet, α 9 α 10P198, which alters the backbone conformation with respect to α 3I196.

The binding of escitalopram to non-orthosteric sites at h(α 3)₃(β 4)₂ is fairly different to that described above for the orthosteric sites. However, none of these differences seem to be essential to explain the absence of this type of binding at the h(α 9)₂(α 10)₃ AChR. At the (+) β 4 side, however, R151 forms a cation- π interaction that might be indispensable for escitalopram binding, that is lacking at α 9 and α 10 where G149 is the homologous residue.

4. Discussion

This work demonstrates the selectivity of (\pm)-citalopram for different AChR subtypes, the different mechanisms of inhibition between α 9 α 10 AChRs and native α 3 β 4* AChRs expressed in MHb (VI) neurons, and whether this antidepressant shares the same binding site(s) as that for imipramine.

The present Ca²⁺ influx results indicate the following AChR selectivity for (\pm)-citalopram (IC₅₀s in μ M): h α 3 β 4 (5.1 \pm 1.3) > h α 7 (18.8 \pm 1.1) ~ h α 4 β 2 (19.1 \pm 4.2). Interestingly, the same preference for h α 3 β 4 AChRs was observed for other SSRIs (Arias et al., 2010a) as well as for structurally different antidepressants such as tricyclic antidepressants (Arias et al., 2018b, 2010b; 2010c) and bupropion (Arias et al., 2018a, 2014) using the same assay (i.e., Ca²⁺ influx). Based on previous studies of several SSRIs at h α 3 β 4 AChRs (Arias et al., 2010a), the following rank order of inhibitory potencies was obtained: fluoxetine (2.0 \pm 0.4) ~ paroxetine (2.6 \pm 0.3) > (\pm)-citalopram (5.1 \pm 1.3).

Our competition binding results indicated that (\pm)-citalopram inhibits [³H]imipramine binding to desensitized h α 3 β 4 AChRs with > 2-fold higher affinity than that for desensitized h α 4 β 2 AChRs. By comparing with other SSRIs (Arias et al., 2010a), the following rank order of affinities (K_i's in μ M) for the h α 3 β 4 AChR was obtained: (\pm)-citalopram (1.8 \pm 0.1) > fluoxetine (4.8 \pm 0.5) > paroxetine (6.9 \pm 0.6), indicating that although (\pm)-citalopram binds with relatively higher affinity to its allosteric h α 3 β 4 AChR sites, its cellular response is less efficient compared to that for other used SSRIs.

The results from a variety of methods coincide with a luminal location for citalopram's binding site(s) at habenular α 3 β 4* AChRs. First, the patch-clamp results demonstrated that (\pm)-citalopram inhibits ACh-evoked currents in MHb (VI) neurons with relatively high potency (7.6 \pm 1.0 μ M) in a voltage-dependent manner, by interacting with a binding site located close to the middle portion of the ion channel [i.e., electrical distance (δ) = 0.40]. Second, the molecular docking and *in silico* results using the h(α 3)₃(β 4)₂ model showed two luminal sites for escitalopram, compatible with an ion channel blockade mechanism. Interestingly, the high-affinity luminal site for escitalopram where β 4-F255 is crucial was situated between positions 5' and 16', in agreement with the calculated electrical distance and at the same level of the imipramine locus within the α 3 β 4 ion channel found in previous studies (Arias et al., 2010a). Since our radioligand binding results showed direct competition between [³H]imipramine and (\pm)-citalopram, we can conclude that citalopram isomers overlap the binding site for imipramine. Given that the high-affinity site for citalopram is located in the middle of the ion channel compared to the low-affinity site, which is closer to the cytoplasmic side of the ion channel, a potential scenario can be considered where once the high-affinity site is occupied by citalopram, the probability of the low-affinity site to be occupied is considerably diminished. This mutually exclusive mechanism is

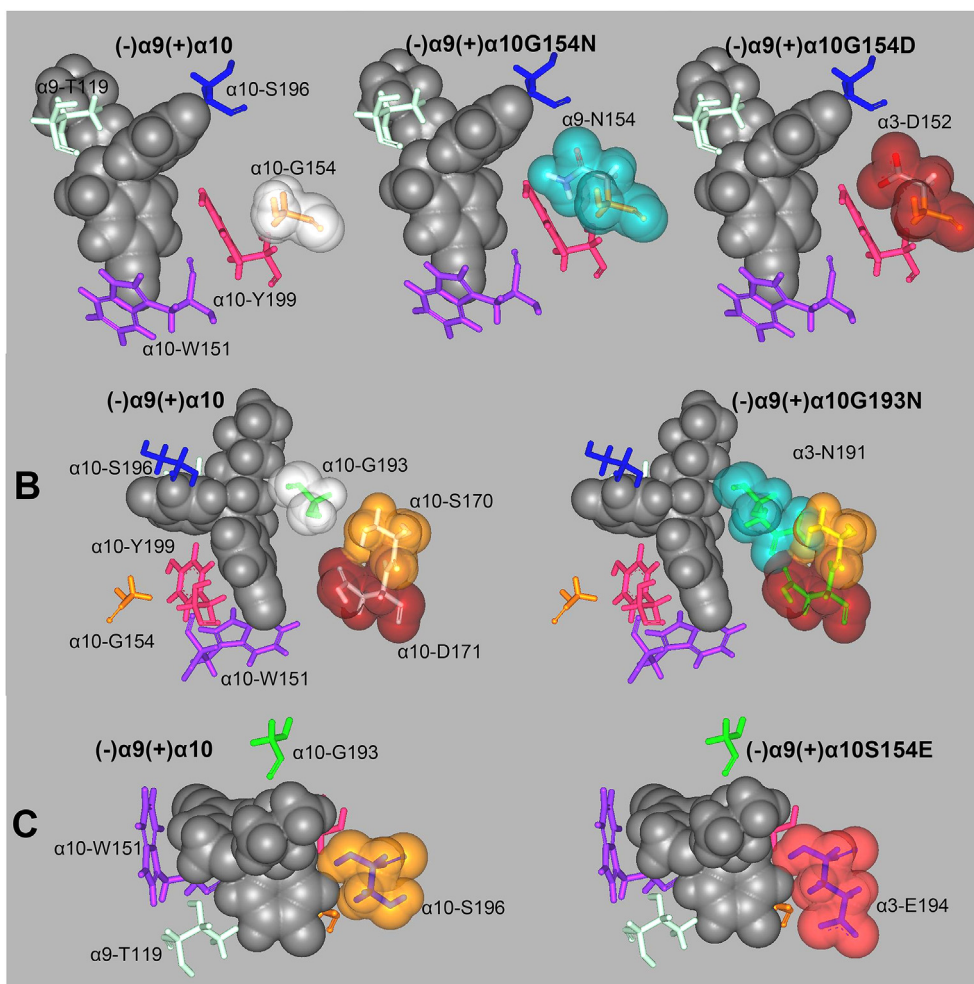


Fig. 7. *In silico* mutations of (+)α10 residues involved in escitalopram binding to orthosteric sites to their respective homologous residues at α9 and α3. (A) α10-G154 mutations to its α9 (α10G154N) and α3 (α10G154D) homologous residues. (B) α10-G193 mutation to its α3 homologous residue (α10G193N). (C) α10-S196 mutation to its α3 homologous residue (α10S196E). Escitalopram is represented by its van der Waal solid surface in black. Mutated residues are represented as sticks surrounded by their van der Waal transparent surfaces. Other important binding site residues are represented as sticks.

compatible with the observed n_H value close to unity, suggesting a non-cooperative mechanism.

The majority of the current response at Mhb (VI) neurons has been ascribed to α3β4* AChRs (Quick et al., 1999; Shih et al., 2014), strongly suggesting that the observed inhibition is mediated by this receptor subtype. Interestingly, this value is similar to that obtained by Ca^{2+} influx experiments where (±)-citalopram inhibits HEK293- $h\alpha3\beta4$ cells expressing only the $h\alpha3\beta4$ AChR subtype. Although a direct comparison of the calculated potencies between heterologous cells and Mhb (VI) neurons cannot be done due to intrinsic differences in the used methods [e.g., see (Arias et al., 2018b, 2017)], it is possible to suggest that (±)-citalopram inhibits a homogenous population of α3β4* AChRs in Mhb (VI) neurons. These results contrast with that obtained with (+)-catharanthine and (±)-18-methoxyconaridine which apparently inhibit a heterogeneous population of α3β4* AChRs (Arias et al., 2017). Since the mouse brain concentration of R(-)- and S-(+)-citalopram (i.e., escitalopram) after acute treatment with 10 mg/kg (±)-citalopram was 0.5 and 1.1 μM, respectively (Karlsson et al., 2013), it is plausible that part of its clinical activity is mediated by inhibition of habenular α3β4* AChRs.

The voltage-clamp results also demonstrated that (±)-citalopram inhibits ACh-evoked α9α10 currents ($7.5 \pm 0.9 \mu M$) in a voltage-independent and competitive manner. Previous studies showed that imipramine (Arias et al., 2018b) and the serotonergic antagonist ICS-205,930 (Rothlin et al., 2003) inhibited α9α10 AChRs by a competitive

mechanism. These results add to a wide variety of compounds that block α9α10 AChRs with different potencies (Rothlin et al., 2000, 1999; Verbitsky et al., 2000), and support the notion that structurally and functionally different antidepressants inhibit α9α10 AChRs by a competitive mechanism, opposite to the noncompetitive mechanism observed at other AChR subtypes. The molecular docking studies also supported the experimental results indicating a competitive mechanism of inhibition for (±)-citalopram. In particular, escitalopram formed three stable interactions with orthosteric, but not luminal, sites at the $h(\alpha9)_2(\alpha10)_3$ AChR, which is compatible with the observed n_H value greater than unity, suggesting a cooperative mechanism between multiple sites. *In silico* mutations also showed that the β9-β10 loop (i.e., “loop C”, which carries the characteristic double Cys in the α subunits) is fundamental for orthosteric binding to $h(\alpha9)_2(\alpha10)_3$, whereas alterations in the loop conformation, especially on α10R186 and α10P198 homologous positions, are responsible for the lack of orthosteric binding to $h(\alpha3)_3(\beta4)_2$.

The results indicating that (±)-citalopram has higher selectivity for α3β4 AChRs and inhibits habenular α3β4* AChRs could be related to its clinical effects. This possibility is based on the observed relationship that compounds with relatively higher selectivity for α3β4 AChRs such as bupropion and mecamylamine present antidepressant activity (Arias et al., 2018a, 2014). The observation that the same compounds act in a synergistic manner with 18-methoxyconaridine (Glick et al., 2002) and all of them alleviate alcohol and nicotine

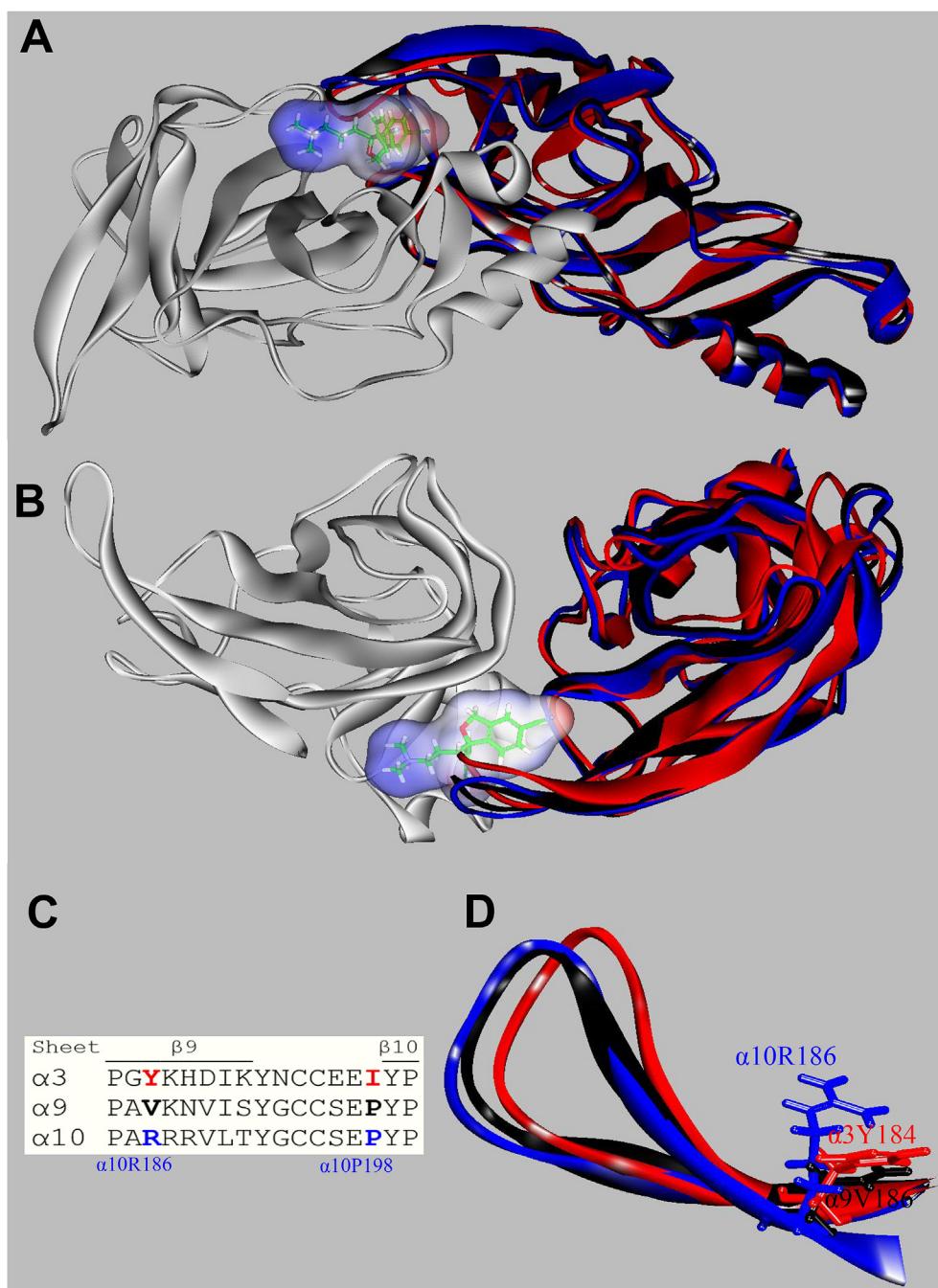


Fig. 8. Orthosteric binding sites at the superposed (+)α3 (red), (+)α9 (black), (+)α10 (blue), and (-)α9 (white) subunits. Escitalopram is shown as sticks surrounded by its molecular surface. The β9-β10 loop at the α3 and α9 subunits are closer to the receptor center than that at α10 (A: Extracellular view; B: Cytoplasmic view), and consequently there is no room for escitalopram to fit in the agonist binding site in α3 and α9. The α3- and α9-β9-β10 loops overlap the ligand when is docked as in the (α9)₂(α10)₃ receptor. (C) Amino acid sequence comparison between α3, α9, and α10 subunits at the level of the β9-β10 loop. Blue: amino acids identified as the cause of the different β9-β10 loop conformations (see text). (D) A detailed side chain view at α10R186, α9V186, and α3Y184 positions, showing the differences of side chains occupied volume that would force the α10-β9-β10 loop to set apart from the receptor.

withdrawal effects (Arias et al., 2014; Chi and De Wit, 2003), might be related with the beneficial effects elicited by (±)-citalopram during alcohol withdrawal (Angelone et al., 1998).

Our findings clearly demonstrate that (±)-citalopram presents receptor selectivity, preferably inhibiting α3β4 and α9α10 AChRs but by different mechanisms. The results showing that (±)-citalopram inhibits MHb (VI) neurons with potency similar to that found at hα3β4 AChRs support that concept that this antidepressant interacts with a homogeneous population of native α3β4* AChRs.

Acknowledgements

This work was supported by grants from NIH (DA040626) (to R.M.D.), National Agency for Scientific and Technologic Promotion, Argentina (to A.B.E.), and Dirección General de Asuntos del Personal Académico, UNAM, Mexico (PASPA grant) (to J.G-C) and Oklahoma

State University (to H.R.A.).

References

- Andreasen, J.T., Henningsen, K., Bate, S., Christiansen, S., Wiborg, O., 2011a. Nicotine reverses anhedonic-like response and cognitive impairment in the rat chronic mild stress model of depression: comparison with sertraline. *J. Psychopharmacol.* <https://doi.org/10.1177/0269881110391831>.
- Andreasen, J.T., Nielsen, E.O., Christensen, J.K., Olsen, G.M., Peters, D., Mirza, N.R., Redrobe, J.P., 2011b. Subtype-selective nicotinic acetylcholine receptor agonists enhance the responsiveness to citalopram and reboxetine in the mouse forced swim test. *J. Psychopharmacol.* <https://doi.org/10.1177/0269881110364271>.
- Andreasen, J.T., Redrobe, J.P., Nielsen, E.O., 2012. Combined α7 nicotinic acetylcholine receptor agonism and partial serotonin transporter inhibition produce antidepressant-like effects in the mouse forced swim and tail suspension tests: a comparison of SSR180711 and PNU-282987. *Pharmacol. Biochem. Behav.* <https://doi.org/10.1016/j.pbb.2011.11.004>.
- Angelone, S.M., Bellini, L., Di Bella, D., Catalano, M., 1998. Effects of fluvoxamine and citalopram in maintaining abstinence in a sample of Italian detoxified alcoholics.

- Alcohol Alcohol. <https://doi.org/10.1093/oxfordjournals.alcalca.a008371>.
- Arias, H.R., Biala, G., Ślomka, K., Targowska-Duda, K.M., Biala, G., Kruk-Ślomka, M., 2014. Interaction of nicotinic receptors with bupropion: structural, functional, and pre-clinical perspectives. *Recept. Clin. Investig.* 1, 30–45. <https://doi.org/10.14800/rci.65>.
- Arias, H.R., Feuerbach, D., Ortells, M.O., 2018a. Bupropion and (±)-SADU-3-72 inhibit human $\alpha 3\beta 4$ nicotinic acetylcholine receptors by luminal and non-luminal interactions. *NeuroTransmitter* e1631. <https://doi.org/10.14800/nt.1631>.
- Arias, H.R., Feuerbach, D., Ortells, M.O., 2016. Bupropion and its photoreactive analog (±)-SADU-3-72 interact with luminal and non-luminal sites at human $\alpha 3\beta 2$ nicotinic acetylcholine receptors. *Neurochem. Int.* 100, 67–77. <https://doi.org/10.1016/j.neuint.2016.08.013>.
- Arias, H.R., Feuerbach, D., Targowska-Duda, K.M., Russell, M., Jozwiak, K., 2010a. Interaction of selective serotonin reuptake inhibitors with neuronal nicotinic acetylcholine receptors. *Biochemistry* 49, 5734–5742. <https://doi.org/10.1021/bi100536t>.
- Arias, H.R., Jin, X., Feuerbach, D., Drenan, R.M., 2017. Selectivity of coronaridine congeners at nicotinic acetylcholine receptors and inhibitory activity on mouse medial habenula. *Int. J. Biochem. Cell Biol.* 92, 202–209. <https://doi.org/10.1016/j.biocel.2017.10.006>.
- Arias, H.R., Rosenberg, A., Targowska-Duda, K.M., Feuerbach, D., Jozwiak, K., Moaddel, R., Wainer, I.W., 2010b. Tricyclic antidepressants and mecamylamine bind to different sites in the human $\alpha 3\beta 2$ nicotinic receptor ion channel. *Int. J. Biochem. Cell Biol.* 42, 1007–1018. <https://doi.org/10.1016/j.biocel.2010.03.002>.
- Arias, H.R., Targowska-Duda, K.M., Feuerbach, D., Sullivan, C.J., Maciejewski, R., Jozwiak, K., 2010c. Different interaction between tricyclic antidepressants and mecamylamine with the human $\alpha 3\beta 4$ nicotinic acetylcholine receptor ion channel. *Neurochem. Int.* 56, 642–649. <https://doi.org/10.1016/j.neuint.2010.01.011>.
- Arias, H.R., Vázquez-Gómez, E., Hernández-Abrego, A., Gallino, S., Feuerbach, D., Ortells, M.O., Elgoyhen, A.B., García-Colunga, J., 2018b. Tricyclic antidepressants inhibit hippocampal $\alpha 7^*$ and $\alpha 9\alpha 10$ nicotinic acetylcholine receptors by different mechanisms. *Int. J. Biochem. Cell Biol.* 100. <https://doi.org/10.1016/j.biocel.2018.04.017>.
- Ballesterro, J.A., Plazas, P.V., Kracun, S., Gomez-Casati, M.E., Taranda, J., Rothlin, C.V., Katz, E., Millar, N.S., Elgoyhen, A.B., 2005. Effects of quinine, quinidine, and chloroquine on $\alpha 9\alpha 10$ nicotinic cholinergic receptors. *Mol. Pharmacol.* 68, 822–829. <https://doi.org/10.1124/mol.105.014431.fusion>.
- Boffi, J.C., Marcovich, I., Gill-Thind, J.K., Corradi, J., Collins, T., Lipovsek, M.M., Moglie, M., Plazas, P.V., Craig, P.O., Millar, N.S., Bouzat, C., Elgoyhen, A.B., 2017. Differential contribution of subunit interfaces to $\alpha 9 \alpha 10$ nicotinic acetylcholine receptor function. *Mol. Pharmacol.* <https://doi.org/10.1124/mol.116.107482>.
- Brejč, K., Van Dijk, W.J., Klaassen, R.V., Schuurmans, M., Van Der Oost, J., Smit, A.B., Sixma, T.K., 2001. Crystal structure of an ACh-binding protein reveals the ligand-binding domain of nicotinic receptors. *Nature*. <https://doi.org/10.1038/35077011>.
- Cheng, Y.-C., Prusoff, W.H., 1973. Relationship between the inhibition constant (K1) and the concentration of inhibitor which causes 50 per cent inhibition (I50) of an enzymatic reaction. *Biochem. Pharmacol.* 22, 3099–3108. [https://doi.org/10.1016/0006-2952\(73\)90196-2](https://doi.org/10.1016/0006-2952(73)90196-2).
- Chi, H., De Wit, H., 2003. Mecamylamine attenuates the subjective stimulant-like effects of alcohol in social drinkers. *Alcohol Clin. Exp. Res.* <https://doi.org/10.1097/01.ALC.0000065435.12068.24>.
- Christmas, D.M., Potokar, J.P., Davies, S.J.C., 2011. A biological pathway linking inflammation and depression: activation of indoleamine 2,3-dioxygenase. *Neuropsychiatric Dis. Treat.*
- Elgoyhen, A.B., Vetter, D.E., Katz, E., Rothlin, C.V., Heinemann, S.F., Boulter, J., 2001. $\alpha 10$: a determinant of nicotinic cholinergic receptor function in mammalian vestibular and cochlear mechanosensory hair cells. *Proc. Natl. Acad. Sci. U. S. A.* 98, 3501–3506. <https://doi.org/10.1073/pnas.051622798>.
- Elgoyhen, A.B., Johnson, D.S., Boulter, J., Vetter, D.E., Heinemann, S., 1994. $\alpha 9$: an acetylcholine receptor with novel pharmacological properties expressed in rat cochlear hair cells. *Cell* 79, 705–715. [https://doi.org/10.1016/0092-8674\(94\)90555-X](https://doi.org/10.1016/0092-8674(94)90555-X).
- Elgoyhen, A.B., Katz, E., 2012. The efferent medial olivocochlear-hair cell synapse. *J. Physiol. Paris* 106, 47–56. <https://doi.org/10.1016/j.jphysparis.2011.06.001>.
- Fryer, J.D., Lukas, R.J., 1999. Antidepressants noncompetitively inhibit nicotinic acetylcholine receptor function. *J. Neurochem.* <https://doi.org/10.1046/j.1471-4159.1999.0721117.x>.
- García-Colunga, J., Awad, J.N., Mileli, R., 1997. Blockage of muscle and neuronal nicotinic acetylcholine receptors by fluoxetine (Prozac). *Proc. Natl. Acad. Sci.* 94, 2041–2044. <https://doi.org/10.1073/pnas.94.5.2041>.
- García-Colunga, J., Targowska-Duda, K.M., Arias, H.R., 2016. Functional and structural interactions between selective serotonin reuptake inhibitors and nicotinic acetylcholine receptors. *NeuroTransmitter* 3, 1293. <https://doi.org/10.14800/nt.1293>.
- Glick, S.D., Maisonneuve, I.M., Kitchen, B.A., 2002. Modulation of nicotine self-administration in rats by combination therapy with agents blocking $\alpha 3\beta 4$ nicotinic receptors. *Eur. J. Pharmacol.* [https://doi.org/10.1016/S0014-2999\(02\)01944-1](https://doi.org/10.1016/S0014-2999(02)01944-1).
- Goutman, J.D., Elgoyhen, A.B., Gómez-Casati, M.E., 2015. Cochlear hair cells: the sound-sending machines. *FEBS Lett.* 589, 3354–3361. <https://doi.org/10.1016/j.febslet.2015.08.030>.
- Karlsson, L., Carlsson, B., Hiemke, C., Ahlner, J., Bengtsson, F., Schmitt, U., Kugelberg, F.C., 2013. Altered brain concentrations of citalopram and escitalopram in P-glycoprotein deficient mice after acute and chronic treatment. *Eur. Neuropsychopharmacol.* 23, 1636–1644. <https://doi.org/10.1016/j.euroneuro.2013.01.003>.
- Maisonneuve, I.M., Glick, S.D., 2003. Anti-addictive actions of an iboga alkaloid congener: a novel mechanism for a novel treatment. *Pharmacol. Biochem. Behav.* [https://doi.org/10.1016/S0091-3057\(03\)00119-9](https://doi.org/10.1016/S0091-3057(03)00119-9).
- McCallum, S.E., Cowe, M.A., Lewis, S.W., Glick, S.D., 2012. $\alpha 3\beta 4$ nicotinic acetylcholine receptors in the medial habenula modulate the mesolimbic dopaminergic response to acute nicotine in vivo. *Neuropharmacology.* <https://doi.org/10.1016/j.neuropharm.2012.04.015>.
- McIntosh, J.M., Absalom, N., Chebib, M., Elgoyhen, A.B., Vincler, M., 2009. $\alpha 9$ nicotinic acetylcholine receptors and the treatment of pain. *Biochem. Pharmacol.* <https://doi.org/10.1016/j.bcp.2009.05.020>.
- Mineur, Y.S., Picciotto, M.R., 2010. Nicotine receptors and depression: revisiting and revising the cholinergic hypothesis. *Trends Pharmacol. Sci.* 31, 580–586. <https://doi.org/10.1016/j.tips.2010.09.004>.
- Morales-Perez, C.L., Noviello, C.M., Hibbs, R.E., 2016. X-ray structure of the human $\alpha 4\beta 2$ nicotinic receptor. *Nature* 538. <https://doi.org/10.1038/nature19785>.
- Morley, B.J., Whiteaker, P., Elgoyhen, A.B., 2018. Commentary: nicotinic acetylcholine receptor $\alpha 9$ and $\alpha 10$ subunits are expressed in the brain of mice. *Front. Cell. Neurosci.* <https://doi.org/10.3389/fncel.2018.00104>.
- Pedretti, A., Villa, L., Vistoli, G., 2004. VEGA - an open platform to develop chemoinformatics applications, using plug-in architecture and script programming. *J. Comput. Aided Mol. Des.* 18, 167–173. <https://doi.org/10.1023/B:JCAM.0000035186.90683.f2>.
- Peng, H., Ferris, R.L., Matthews, T., Hiel, H., Lopez-Albaitero, A., Lustig, L.R., 2004. Characterization of the human nicotinic acetylcholine receptor subunit alpha (α) 9 (CHRNA9) and alpha (α) 10 (CHRNA10) in lymphocytes. *Life Sci.* <https://doi.org/10.1016/j.lfs.2004.05.031>.
- Phillips, J.C., Braun, R., Wang, W., Gumbart, J., Tajkhorshid, E., Villa, E., Chipot, C., Skeel, R.D., Kalé, L., Schulten, K., 2005. Scalable molecular dynamics with NAMD. *J. Comput. Chem.* 26, 1781–1802. <https://doi.org/10.1002/jcc.20289>.
- Plazas, P.V., Katz, E., Gomez-Casati, M.E., Bouzat, C., Elgoyhen, A.B., 2005. Stoichiometry of the $\alpha 9\alpha 10$ nicotinic cholinergic receptor. *J. Neurosci.* <https://doi.org/10.1523/JNEUROSCI.3805-05.2005>.
- Popik, P., Kozela, E., Krawczyk, M., 2003. Nicotine and nicotinic receptor antagonists potentiate the antidepressant-like effects of imipramine and citalopram. *Br. J. Pharmacol.* <https://doi.org/10.1038/sj.bjp.0705359>.
- Quick, M.W., Ceballos, R.M., Kasten, M., McIntosh, J.M., Lester, R.A.J., 1999. $\alpha 3\beta 4$ subunit-containing nicotinic receptors dominate function in rat medial habenula neurons. *Neuropharmacology.* [https://doi.org/10.1016/S0028-3908\(99\)00024-6](https://doi.org/10.1016/S0028-3908(99)00024-6).
- Rezvani, A.H., Cauley, M.C., Slade, S., Wells, C., Glick, S., Rose, J.E., Levin, E.D., 2016. Acute oral 18-methoxycoronaridine (18-MC) decreases both alcohol intake and IV nicotine self-administration in rats. *Pharmacol. Biochem. Behav.* <https://doi.org/10.1016/j.pbb.2016.10.010>.
- Romero, H.K., Christensen, S.B., Di Cesare Mannelli, L., Gajewiak, J., Ramachandra, R., Elmslie, K.S., Vetter, D.E., Ghelardini, C., Iadonato, S.P., Mercado, J.L., Olivera, B.M., McIntosh, J.M., 2017. Inhibition of $\alpha 9\alpha 10$ nicotinic acetylcholine receptors prevents chemotherapy-induced neuropathic pain. *Proc. Natl. Acad. Sci.* 114, E1825–E1832. <https://doi.org/10.1073/pnas.1621433114>.
- Rothlin, C.V., Katz, E., Verbitsky, M., Vetter, D.E., Heinemann, S.F., Elgoyhen, A.B., 2000. Block of the $\alpha 9$ nicotinic receptor by ototoxic aminoglycosides. *Neuropharmacology.* [https://doi.org/10.1016/S0028-3908\(00\)00056-3](https://doi.org/10.1016/S0028-3908(00)00056-3).
- Rothlin, C.V., Lioudyno, M.I., Silbering, A.F., Plazas, P.V., Casati, M.E., Katz, E., Guth, P.S., Elgoyhen, A.B., 2003. Direct interaction of serotonin type 3 receptor ligands with recombinant and native $\alpha 9\alpha 10$ -containing nicotinic cholinergic receptors. *Mol. Pharmacol.* <https://doi.org/10.1124/mol.63.5.1067>.
- Rothlin, C.V., Katz, E., Verbitsky, M., Elgoyhen, A.B., 1999. The $\alpha 9\alpha 10$ nicotinic acetylcholine receptor shares pharmacological properties with type A gamma-aminobutyric acid, glycine, and type 3 serotonin receptors. *Mol. Pharmacol.*
- Sacre, S., Medghalchi, M., Gregory, B., Brennan, F., Williams, R., 2010. Fluoxetine and citalopram exhibit potent antiinflammatory activity in human and murine models of rheumatoid arthritis and inhibit toll-like receptors. *Arthritis Rheum.* <https://doi.org/10.1002/art.27304>.
- Šali, A., Potterton, L., Yuan, F., van Vlijmen, H., Karplus, M., 1995. Evaluation of comparative protein modeling by MODELLER. *Proteins Struct. Funct. Bioinforma.* <https://doi.org/10.1002/prot.340230306>.
- Shih, P.-Y., Engle, S.E., Oh, G., Deshpande, P., Puskar, N.L., Lester, H.A., Drenan, R.M., 2014. Differential expression and function of nicotinic acetylcholine receptors in subdivisions of medial habenula. *J. Neurosci.* <https://doi.org/10.1523/JNEUROSCI.0476-14.2014>.
- Stein, D.J., Montgomery, S.A., Kasper, S., Tanghoj, P., 2001. Predictors of response to pharmacotherapy with citalopram in obsessive-compulsive disorder. *Int. Clin. Psychopharmacol.* <https://doi.org/10.1097/00004850-200111000-00007>.
- Trott, O., Olson, A.J., 2010. Software news and update AutoDock Vina: improving the speed and accuracy of docking with a new scoring function, efficient optimization, and multithreading. *J. Comput. Chem.* 31, 455–461. <https://doi.org/10.1002/jcc.21334>.
- Varia, I., Rauscher, F., 2002. Treatment of generalized anxiety disorder with citalopram. *Int. Clin. Psychopharmacol.*
- Verbitsky, M., Rothlin, C.V., Katz, E., Belén Elgoyhen, A., 2000. Mixed nicotinic-muscarinic properties of the $\alpha 9$ nicotinic cholinergic receptor. *Neuropharmacology.* [https://doi.org/10.1016/S0028-3908\(00\)00124-6](https://doi.org/10.1016/S0028-3908(00)00124-6).